

The Hunt for the Rest of the Higgs Bosons

Nathaniel Craig,^a Francesco D'Eramo,^{b,c} Patrick Draper,^a Scott Thomas,^d and Hao Zhang^a

^a*Department of Physics, University of California, Santa Barbara, CA 93106, USA*

^b*Department of Physics, University of California, Berkeley, CA 94720 USA*

^c*Theoretical Physics Group, Lawrence Berkeley National Laboratory, Berkeley, CA 94720, USA*

^d*Department of Physics and Astronomy, Rutgers University, Piscataway, NJ 08854, USA*

E-mail: ncraig@physics.ucsb.edu, fraderamo@berkeley.edu,
pidraper@physics.ucsb.edu, scthomas@physics.rutgers.edu,
zhanghao@physics.ucsb.edu

ABSTRACT: We assess the current state of searches at the LHC for additional Higgs bosons in light of both direct limits and indirect bounds coming from coupling measurements of the Standard Model-like Higgs boson. Given current constraints, we identify and study three LHC searches that are critical components of a comprehensive program to investigate extended electroweak symmetry breaking sectors: production of a heavy scalar or pseudoscalar with decay to $t\bar{t}$; $b\bar{b}$ and $t\bar{t}$ associated production of a heavy scalar or pseudoscalar with decay to invisible final states; and $t\bar{b}$ associated production of a charged Higgs with decay to $\bar{t}b$. Systematic experimental searches in these channels would contribute to robust coverage of the possible single production modes of additional heavy Higgs bosons.

ARXIV EPRINT: [15xx.xxxxx](https://arxiv.org/abs/15xx.xxxxx)

Contents

1	Introduction	1
2	Direct and Indirect 2HDM Limits	4
3	Searching for a Neutral Higgs in $t\bar{t}$	13
3.1	$pp \rightarrow H/A \rightarrow t\bar{t}$	14
3.2	$pp \rightarrow b\bar{b}H/A \rightarrow b\bar{b}t\bar{t}$ and $pp \rightarrow t\bar{t}H/A \rightarrow t\bar{t}t\bar{t}$	17
4	Searching for an Invisible Neutral Higgs	20
4.1	Models with $H/A \rightarrow \cancel{E}_T$	21
4.2	$b\bar{b} + \cancel{E}_T$ at 8 TeV	22
4.3	$t\bar{t} + \cancel{E}_T$ at 14 TeV	24
5	Searching for a Charged Higgs in $t\bar{b}$	26
6	Conclusions	29
A	Higgs Couplings Fit	30
B	The $gg \rightarrow H/A \rightarrow t\bar{t}$ Differential Cross Section	33
C	Top Quark Reconstruction	36

1 Introduction

Following the discovery of a Standard Model-like Higgs boson at the LHC, the systematic search for additional weakly-coupled scalars near the electroweak scale is of paramount importance. A variety of experimental searches have been performed for such extended Higgs sectors to date, predominantly targeting new scalars with substantial couplings to the electroweak gauge bosons [1–7] or to down-type fermions [8, 9]. However, these searches are only sensitive to a fraction of the interesting parameter space in general extended Higgs sectors. This raises the surprising possibility that a large number of additional Higgs bosons have been produced at the LHC without leaving signals in existing search channels.

Moving forward into Run 2 at the LHC, a natural question is *how the search for additional Higgses should be organized* in order to ensure systematic coverage of extended electroweak symmetry breaking sectors. Given the proliferation of potential signals, it is useful to consider signatures broadly. Interesting topologies and searches for new Higgs bosons can be

classified in terms of simplified models, much in the spirit of simplified model searches for supersymmetry [10–12]. These simplified models may then be combined to provide coverage of the parameter space of a given extended Higgs sector.

A useful first step in organizing the search for additional states is to begin with the signatures of a single additional Higgs boson, so that the available decay modes involve Standard Model (SM) bosons and fermions, the 125 GeV Higgs, and potentially additional invisible decays. In a general extended Higgs sector there may be numerous Higgs bosons beyond the SM Higgs. By focusing on one new state at a time, we can characterize the dominant signals of an extended Higgs sector if the additional Higgs bosons are well separated in mass, or if the additional Higgs bosons are approximately degenerate so that decays between heavy Higgs bosons are kinematically disfavored. Having comprehensively covered these signatures, it is then possible to systematically expand the picture to consider production and decay processes involving more than one heavy Higgs boson.

Within the space of signatures of a single new Higgs state, further powerful guidance is provided by the coupling measurements of the recently-discovered SM-like Higgs boson, which constrain the parameter space of extended Higgs sectors. These coupling measurements are currently consistent with SM predictions to within the 20–30% level. Such agreement suggests that any extension of the Higgs sector must be near an *alignment limit* in its parameter space, wherein the SM-like Higgs boson is closely aligned with the vacuum expectation value (vev) that breaks electroweak symmetry and correspondingly exhibits the properties of a SM Higgs boson [13–16]. In a given extended Higgs sector, this alignment limit may be approached either due to decoupling of additional Higgs states [16, 17], or simply due to the organization of dimensionless couplings in the Higgs potential [13–15, 18–20]. Proximity to the alignment limit then governs also the couplings of additional Higgs bosons, and may be used as a guide to searches for additional Higgses.

The precise properties of the SM-like Higgs boson and additional Higgs scalars near the alignment limit depend on the nature of the extended Higgs sector. The SM Higgs boson is a *vacuum state* in that it carries the quantum numbers of the vacuum. Additional neutral Higgs bosons may include *pure vacuum states* with the quantum numbers of the vacuum, allowing mixing with the SM Higgs, but without intrinsic coupling to gauge bosons or fermions. Mixing with new pure vacuum states modify the SM-like Higgs boson couplings in a model-independent way by diluting all couplings uniformly. The real singlet extension of the Higgs sector provides a natural example of a pure vacuum state, with one new CP-even Higgs boson whose couplings to SM fermions and gauge bosons are uniformly suppressed in the alignment limit. In this case, proximity to the alignment limit implies suppression of all production modes for the additional boson at the LHC.

Alternately, additional neutral Higgs bosons may simply include new *vacuum states* allowing both mixing with the SM-like Higgs *and* independent intrinsic couplings to massive gauge bosons and fermions. Such vacuum states modify the SM-like Higgs boson couplings in a model-dependent way. Such vacuum states arise, for example, in CP-conserving Two-Higgs-Doublet Models (2HDM). The physical spectrum of 2HDM includes four additional

Higgs bosons – a CP-even scalar H , CP-odd pseudoscalar A , and charged Higgs bosons H^\pm , of which the CP-even scalar H without any quantum numbers can be identified as a vacuum state. The couplings of these additional Higgs bosons to SM bosons are suppressed in the alignment limit, while their couplings to SM fermions are generically unsuppressed but depend in detail on the coupling structure of the 2HDM. In this case, proximity to the alignment limit implies suppression of production and decay modes involving SM bosons, while production and decay via SM fermions may be appreciable. Consequently, typical searches such as $H \rightarrow ZZ$ become ineffective. Similarly, $H/A \rightarrow \tau\tau$ and $H^\pm \rightarrow \tau\nu$ searches may be effective in some scenarios, but are ineffective whenever the down-type fermionic couplings are not substantially enhanced over the SM Yukawas.

In this paper we articulate a systematic strategy for searching individually for additional Higgs scalars in light of the properties of the 125 GeV Higgs. We focus on the phenomenology of CP-conserving scenarios with two Higgs doublets satisfying the Glashow-Weinberg (GW) condition [21], as this describes the physics of many well-motivated extensions of the Higgs sector while still covering many of the key features of models with additional singlets or higher electroweak representations. We first summarize the state of limits on 2HDM at the LHC from direct searches for additional Higgs states and indirect constraints from Higgs coupling measurements (for recent related work, see [14, 22–37]). We then identify and study three primary channels where, without being meaningfully constrained by existing searches, a second Higgs boson could exhibit $\mathcal{O}(1)$ signals:

1. The single production of a heavy scalar or pseudoscalar Higgs boson with decay to $t\bar{t}$.
2. The single production of a heavy scalar or pseudoscalar with decay to invisible final states.
3. The tb associated production of a charged Higgs with decay to tb .¹

In each case, “single production” includes both resonant production of a single heavy Higgs boson and potential associated production modes involving SM fermions in conjunction with a heavy Higgs boson. The combination of Higgs coupling measurements, ongoing searches for heavy Higgses, and the three search channels studied in this work should contribute a rather comprehensive coverage of individual scalar states in extended electroweak symmetry breaking sectors.

The paper is organized as follows: In section 2 we first review the constraints from current Higgs coupling measurements on the parameter space of motivated 2HDM, then present the combined impact of existing direct searches for heavy Higgs states on the same parameter space. In section 3 we consider one of the most pressing signatures of additional Higgs scalars in light of current direct and indirect limits: the strong production of a heavy neutral Higgs

¹Although the $H^\pm tb$ process with dileptonic top decay is the subject of a recent CMS search at 8 TeV [38], there is room for improvement in the reach, particularly by inclusion of the semileptonic top decay channel studied here at 14 TeV.

boson followed by decay into $t\bar{t}$. This process has a distinctive interference between signal and SM $t\bar{t}$ background [39], but is hampered by the sizable SM background, and further complicated by the modest reconstruction resolution available at the LHC of the invariant mass of the $t\bar{t}$ system. Given the challenges of the search for resonant $t\bar{t}$ production, we also briefly consider $t\bar{t}$ and $b\bar{b}$ associated production of a heavy neutral Higgs followed by decay to $t\bar{t}$. In section 4 we turn to invisible decays of heavy Higgses. We consider $t\bar{t}$ and $b\bar{b}$ associated production of an invisibly-decaying heavy Higgs boson, as proximity to the alignment limit renders ineffective traditional searches involving vector bosons. Finally, in section 5 we study the $t\bar{b}$ associated production and decay of charged Higgs bosons. We conclude in section 6 and reserve details of our Higgs fit, kinematics of the $H/A \rightarrow t\bar{t}$ process, and top quark reconstruction algorithm for a series of appendices.

2 Direct and Indirect 2HDM Limits

Direct searches at the LHC and indirect limits arising from Higgs coupling measurements impose constraints on the parameter space of 2HDM. As we will discuss in this section, the search for additional Higgses is guided by the complementarity of these direct and indirect constraints.

In light of stringent flavor constraints, we focus on (CP-conserving) 2HDM satisfying the Glashow-Weinberg condition that all fermions of a given representation receive their masses via renormalizable couplings to a single Higgs doublet. There are four distinct possible configurations satisfying the GW condition; in this paper we will further focus on the two most common, known as Type 1 and Type 2 2HDM. In Type 1 2HDM all SM fermions couple to one doublet, while in Type 2 2HDM the up-type quarks and down-type quarks/leptons couple to separate doublets. These two types arise most frequently in motivated extensions of the SM, including composite Higgs models, little Higgs models, and supersymmetric models; the Higgs sector of the MSSM is an instance of the Type 2 2HDM.

In theories with two Higgs doublets Φ_1, Φ_2 and the most general renormalizable CP-conserving potential, there are nine free parameters that remain after minimizing the potential and fixing the symmetry breaking vev $v^2 = v_1^2 + v_2^2 = (246 \text{ GeV})^2$. There are various possible parameterizations. Here we use the conventions of [14], taking for the free parameters the ratio $\tan \beta = |\langle \Phi_2^0 \rangle / \langle \Phi_1^0 \rangle|$, the mixing angle α that diagonalizes the neutral scalar mass matrix, the four physical masses $\{m_h, m_H, m_A, m_{H^\pm}\}$, and the dimensionless couplings $\lambda_{5,6,7}$.

The coupling of the physical states h, H, A, H^\pm to SM fermions and gauge bosons are fully determined by the angles α and β , while the renormalizable couplings involving three or four physical Higgs bosons depend on the additional parameters of the potential. The couplings of physical scalars to SM fermions and gauge bosons as a function of α and β in Type 1 and Type 2 2HDM are summarized in table 1. In this work we will assume that the observed 125 GeV Higgs is the CP-even scalar h with SM-like Higgs couplings, with the additional Higgs scalars H, A, H^\pm parametrically heavier. The case of additional scalars lighter than the 125 GeV Higgs is also quite interesting but qualitatively distinct.

$y_{2\text{HDM}}/y_{\text{SM}}$	Type 1	Type 2
hVV	$s_{\beta-\alpha}$	$s_{\beta-\alpha}$
hQu	$s_{\beta-\alpha} + c_{\beta-\alpha}/t_\beta$	$s_{\beta-\alpha} + c_{\beta-\alpha}/t_\beta$
hQd	$s_{\beta-\alpha} + c_{\beta-\alpha}/t_\beta$	$s_{\beta-\alpha} - t_\beta c_{\beta-\alpha}$
hLe	$s_{\beta-\alpha} + c_{\beta-\alpha}/t_\beta$	$s_{\beta-\alpha} - t_\beta c_{\beta-\alpha}$
HVV	$c_{\beta-\alpha}$	$c_{\beta-\alpha}$
HQu	$c_{\beta-\alpha} - s_{\beta-\alpha}/t_\beta$	$c_{\beta-\alpha} - s_{\beta-\alpha}/t_\beta$
HQd	$c_{\beta-\alpha} - s_{\beta-\alpha}/t_\beta$	$c_{\beta-\alpha} + t_\beta s_{\beta-\alpha}$
HLe	$c_{\beta-\alpha} - s_{\beta-\alpha}/t_\beta$	$c_{\beta-\alpha} + t_\beta s_{\beta-\alpha}$
AVV	0	0
AQu	$1/t_\beta$	$1/t_\beta$
AQd	$-1/t_\beta$	t_β
ALe	$-1/t_\beta$	t_β

Table 1: The coupling of Higgs bosons h, H, A to SM bosons and fermions as a function of the angles α and β , expressed in terms of the alignment parameter $c_{\beta-\alpha} \equiv \cos(\beta - \alpha)$, and $t_\beta \equiv \tan \beta$. The coupling dependence of the charged scalars H^\pm is the same as the pseudo-scalar A .

It is apparent from table 1 that couplings of the CP-even scalar h become exactly SM-like in the limit $\cos(\beta - \alpha) \rightarrow 0$, which coincides with the alignment limit for 2HDM satisfying the Glashow-Weinberg condition. In the alignment limit the heavy CP-even neutral Higgs H decouples from SM vector bosons, and its couplings become akin to those of the pseudoscalar Higgs A . Crucially, the Higgs bosons H, A , and H^\pm retain couplings to SM fermions in the alignment limit. These couplings ensure that the additional states have non-vanishing production channels and visible decay signatures involving SM fermions even in the limit where the 125 GeV Higgs is exactly SM-like.

At present, the SM-like nature of the 125 GeV Higgs boson implies proximity to the alignment limit commensurate with the precision of Higgs coupling measurements. In order to quantify the impact on the (α, β) parameter space of 2HDM, we perform a global fit to recent Higgs measurements reported by the ATLAS and CMS collaborations.² We provide details of our fit procedure in appendix A. In figures 1 we show the result of global fits for Type 1 and Type 2 2HDM as a function of $\tan \beta$ and $\cos(\beta - \alpha)$. We refer the reader to [14] for discussion of the physics underlying the shape of these fits.

The proximity to the alignment limit implied by coupling measurements of the SM-like

²For this fit and for the interpretation of direct searches for heavy Higgs bosons, we use the programs HIGLU/HDECAY [40] to determine the NLO dependence of the $h/H/A$ gluon fusion production cross section and partial widths $h/H \rightarrow gg, t\bar{t}, b\bar{b}, s\bar{s}, c\bar{c}, \mu\mu, \tau\tau, WW, ZZ$, and $A \rightarrow gg$ on the parameters α and β . We use analytic NLO QCD expressions for the partial widths $h/H/A \rightarrow \gamma\gamma$ [41] and $A \rightarrow t\bar{t}, b\bar{b}, c\bar{c}$ [42, 43]. We use the program SUSHI [44] to determine the NLO $b\bar{b}h/H/A$ production cross section and validate the HIGLU result for gluon fusion. We use MadGraph 5 [45] to determine the LO $t\bar{t}h/H/A$ production cross section with a k -factor of 1.18 [46]. We use leading order results for the partial widths $H \rightarrow hh$ and $A \rightarrow Zh, \tau\tau, \mu\mu$ [47].

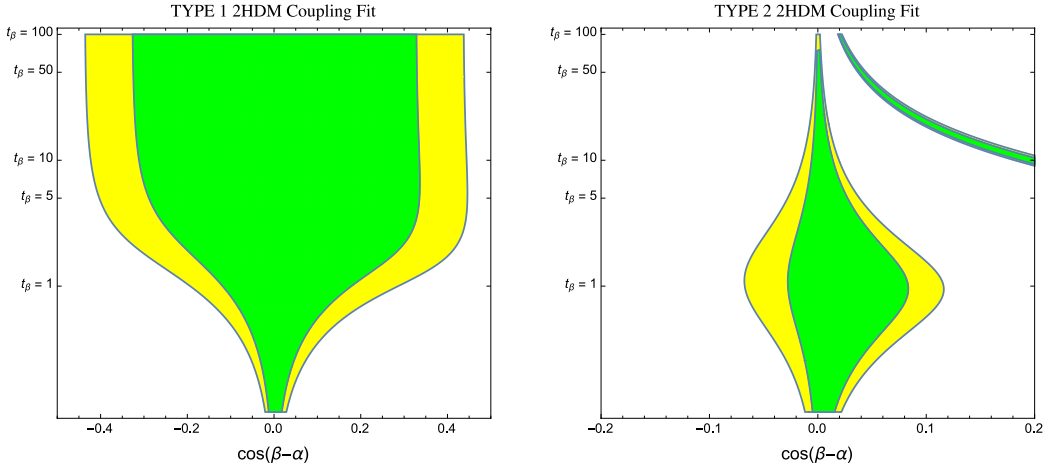


Figure 1: Coupling fits in the 2HDM parameter space of $\tan\beta$ and $\cos(\beta - \alpha)$ in Type 1 (left) and Type 2 (right) 2HDM. Details of the fit procedure are discussed in appendix A.

Higgs provides a natural organizing principle for the signatures of additional Higgs bosons. The implications for production modes are particularly transparent. In Type 1 2HDM, current fits require $\cos(\beta - \alpha) \lesssim 0.4$, suggesting that vector associated production modes of H such as ZH associated production or vector boson fusion (VBF) are suppressed by at least a factor ~ 0.2 relative to a SM Higgs of the same mass. In contrast, strong production modes may remain appreciable. Gluon fusion production of H or A proceeds through fermion loops as in the SM, uniformly proportional to $\cot^2\beta$ in the alignment limit. The same is true of $t\bar{t}H/A$ and $b\bar{b}H/A$ associated production and $t\bar{b}H^\pm$ associated production, indicating that these channels remain promising in the alignment limit of Type 1 2HDM.

In Type 2 2HDM the suppression implied by Higgs coupling fits is even more extreme, such that vector associated production modes of H are at most $\sim 1\%$ of a SM Higgs of the same mass. As in the case of Type 1 2HDM, strong production modes are still appreciable. Gluon fusion production of H and A again proceeds through fermion loops, with the top loop contribution proportional to $\cot^2\beta$ and the bottom loop contribution proportional to $\tan^2\beta$ at leading order in the alignment limit. The $t\bar{t}H/A$ associated production mode again scales as $\cot^2\beta$, while the $b\bar{b}H/A$ associated production mode scales as $\tan^2\beta$. Production of the charged Higgs is a function of both $\tan\beta$ and $\cot\beta$ in the alignment limit.

The impact on branching ratios of heavy Higgs bosons is somewhat more subtle. As discussed in detail in [14], although proximity to the alignment limit implies suppression of couplings to SM bosons, these longitudinally-enhanced partial widths are competing only with relatively small fermionic partial widths. As such, decays into SM bosons may remain appreciable close to the alignment limit. In the exact alignment limit, tree-level decays into massive SM bosons (including the 125 GeV Higgs h) vanish in favor of decays into SM fermions and the massless gauge bosons.³

³We do not consider loop-level decays into massive vector bosons, which are nonzero in the exact alignment

Single Heavy Higgs Strong Production	$\mathcal{O}(g_s^4 \lambda_f^2)$	$gg \rightarrow H, A$
Single Heavy Higgs Associated Strong Production	$\mathcal{O}(g_s^4 \lambda_f^2)$	$gg \rightarrow bbH, bbA, tbH^\pm, ttH, ttA$
Single Heavy Higgs Associated Weak Production	$\mathcal{O}(g_s^2 g_w^4 \lambda_f^2)$	$gq \rightarrow bq' bH^\pm, bq'tH, bq'tA$
Double Heavy Higgs Weak Production	$\mathcal{O}(g_w^4)$	$q\bar{q} \rightarrow HA, HH^\pm, AH^\pm, H^+H^-$
Light + Heavy Higgs Strong Production	$\mathcal{O}(g_s^4 \lambda_f^4)$	$gg \rightarrow hH, hA$
Double Heavy Higgs Strong Production	$\mathcal{O}(g_s^4 \lambda_f^4)$	$gg \rightarrow HH, HA, AA, H^+H^-$

Table 2: Hierarchy of heavy Higgs leading LHC production channels that do not vanish in the 2HDM alignment limit.

In table 2 we summarize the the leading LHC production channels for heavy Higgs bosons in 2HDM that are non-vanishing in the alignment limit, ordered by their relative size at LHC energies. These include resonant production of heavy neutral Higgses by gluon fusion; single production of heavy neutral or charged Higgses in association with top and bottom quarks; heavy Higgs pair production via Drell-Yan processes; heavy-light Higgs boson production via gluon fusion; and heavy Higgs pair production via gluon fusion. Other production modes that vanish in the alignment limit are *significantly* suppressed near the alignment limit, rendering them unpromising in the parameter space currently allowed by Higgs coupling fits. We likewise summarize the Standard Model decay channels of heavy Higgs bosons in table 3. In contrast with production modes, decay modes that vanish near the alignment limit may still be appreciable near the alignment limit, given the relatively small partial widths of competing decays.

Given proximity to the alignment limit, there is a natural ordering of searches for additional Higgs bosons obtained by combining the dominant production and decay modes. Many of the single heavy Higgs boson production channels are covered by existing searches, including searches for gluon fusion production of H/A with decay to $b\bar{b}, \tau\tau, \gamma\gamma, \mu\mu$ as well as WW, ZZ, Zh, hh ; searches for $b\bar{b}H/A$ associated production with decay to $b\bar{b}, \tau\tau, \mu\mu$; and

limit but sufficiently small to avoid influencing the tree-level result.

		H	A	H^\pm
Standard Model	WW, ZZ	–		
Decay Channels	$tt, bb, \tau\tau, \mu\mu$	✓	✓	
	$\gamma\gamma$	✓	✓	
	Zh		–	
	hh	–		
	Wh			–
	$tb, \tau\nu$			✓

Table 3: Standard Model decay channels of 2HDM heavy Higgs bosons. A checkmark indicates that the partial decay width approaches a constant in the alignment limit, while a dash indicates that the decay width vanishes in the alignment limit.

$t\bar{b}H^\pm$ associated production with decay to $\tau\nu$ and $\bar{t}b$. However, several key channels remain uncovered, particularly gluon fusion with decay to $t\bar{t}$; associated production of $b\bar{b}H/A$ followed by decay to $\gamma\gamma$ and WW, ZZ, Zh, hh as well as $t\bar{t}$; and associated production of $t\bar{t}H/A$ with decay to $b\bar{b}, \tau\tau, \gamma\gamma, \mu\mu$ as well as WW, ZZ, Zh, hh and $t\bar{t}$. Once decay into $t\bar{t}$ becomes kinematically accessible, it becomes one of the primary decay modes of heavy neutral Higgs bosons near the alignment limit, and this decay channel may entirely dominate the visible signatures of additional Higgses. Similarly, $t\bar{b}H^\pm$ associated production with decay to $\bar{t}b$ is likely to be a dominant signature of charged Higgses at the LHC when this decay channel is open. Although there is a search for this mode at $\sqrt{s} = 8$ TeV [38], there is room for improvement in this channel.

In addition to decays into SM final states, it is possible for new Higgs bosons to decay into non-SM final states. These processes include both invisible decays and potentially visible decays that do not fall into the acceptance of existing searches. Given the suppression of vector associated production modes in the alignment limit, the most promising potential channels are $t\bar{t}H/A$ or $b\bar{b}H/A$ associated production with decay to invisible final states.

To fully characterize the state of coverage by direct searches, we interpret searches by the ATLAS and CMS collaborations for heavy Higgs states in the parameter space of Type 1 and Type 2 2HDM. The relevant search channels are summarized in table 4. These searches present limits in terms of single-channel cross sections times branching ratios that are amenable to reinterpretation. Powerful limits on $gg \rightarrow H \rightarrow hh$ and $gg \rightarrow A \rightarrow Zh$ for moderately heavy H, A have also been obtained using multi-lepton and di-photon final states [7], but these bounds combine many exclusive channels with non-uniform scaling and acceptance across the 2HDM parameter space and cannot be easily reinterpreted in our framework.

Channel	Collaboration	Reference
$gg \rightarrow \Phi \rightarrow \gamma\gamma$	ATLAS, 20.3 fb ⁻¹	[48]
$gg \rightarrow \Phi \rightarrow \gamma\gamma$	CMS, 19.7 fb ⁻¹	[49]
$gg \rightarrow \Phi \rightarrow \tau\tau$	ATLAS, 20.3 fb ⁻¹	[8]
$b\bar{b} \rightarrow \Phi \rightarrow \tau\tau$	ATLAS, 20.3 fb ⁻¹	[8]
$gg \rightarrow \Phi \rightarrow \tau\tau$	CMS, 19.7 fb ⁻¹	[9]
$b\bar{b} \rightarrow \Phi \rightarrow \tau\tau$	CMS, 19.7 fb ⁻¹	[9]
$gg \rightarrow A \rightarrow Zh \rightarrow \ell\ell + (b\bar{b}, \tau\tau)$	ATLAS, 20.3 fb ⁻¹	[1]
$gg \rightarrow A \rightarrow Zh \rightarrow \ell\ell + b\bar{b}$	CMS, 19.7 fb ⁻¹	[5]
$gg \rightarrow H \rightarrow hh \rightarrow b\bar{b} + \gamma\gamma$	ATLAS, 20 fb ⁻¹	[50]
$gg \rightarrow H \rightarrow hh \rightarrow b\bar{b} + b\bar{b}$	CMS, 17.9 fb ⁻¹	[51]
$gg \rightarrow H \rightarrow hh \rightarrow b\bar{b} + \gamma\gamma$	CMS, 19.7 fb ⁻¹	[52]
$gg \rightarrow H \rightarrow ZZ \rightarrow 4\ell$	ATLAS, 20.7 fb ⁻¹	[53]
$gg \rightarrow H \rightarrow ZZ$	CMS, 19.7 fb ⁻¹	[6]
$gg \rightarrow H \rightarrow WW$	CMS, 19.7 fb ⁻¹	[6]

Table 4: Relevant ATLAS and CMS searches for heavy Higgs bosons at the $\sqrt{s} = 8$ TeV LHC. Here $\Phi = H, A$.

For each search, we consider the contribution of H or A separately (in contrast to e.g. the MSSM interpretation of searches in the $\tau\tau$ final state, which includes the sum of contributions from h, H , and A). To determine the theory prediction for relevant cross sections times branching ratios across the 2HDM parameter space, we obtain the relevant cross sections and partial widths as a function of α and β as discussed above. Here we assume that the total widths of H and A are determined purely by their decays into SM final states.

In figure 2 we present the state of current direct searches in the exact alignment limit $\cos(\beta - \alpha) = 0$ for heavy CP-even neutral scalar H and CP-odd neutral pseudoscalar A as a function of $\tan\beta$ and $m_{H/A}$ in Type 1 and Type 2 2HDM. In the exact alignment limit, only production and decay modes involving Higgs couplings to fermions (including gluon fusion production and decay into photons arising from top/bottom quark loops) contribute. In Type 1 2HDM all production modes involving fermions are suppressed at large $\tan\beta$, so that existing searches are only effective at low $\tan\beta$. The most sensitive search channels include inclusive production of H/A followed by decay to $\gamma\gamma, \tau\tau$. These channels are modestly effective near $\tan\beta = 1$ for $m_{H/A} \lesssim 350$ GeV, but lose sensitivity for $m_{H/A} \gtrsim 2m_t$ once decays into $t\bar{t}$ go on-shell. In Type 2 2HDM both the gluon fusion and $b\bar{b}H/A$ associated production modes grow at large $\tan\beta$, providing additional sensitivity relative to the Type 1 scenario. Note that the exclusion due to our interpretation of searches in the $\tau\tau$ final state is somewhat weaker than the comparable MSSM exclusion plot. This is due to the fact that the MSSM interpretation combines contributions from h, H , and A , whereas we consider only the contribution due to H or A individually. In both 2HDM types, the profound weakening of limits at low $\tan\beta$ in the alignment limit when the $H/A \rightarrow t\bar{t}$ channel becomes kinematically accessible highlights the need for effective searches in the $t\bar{t}$ final state.

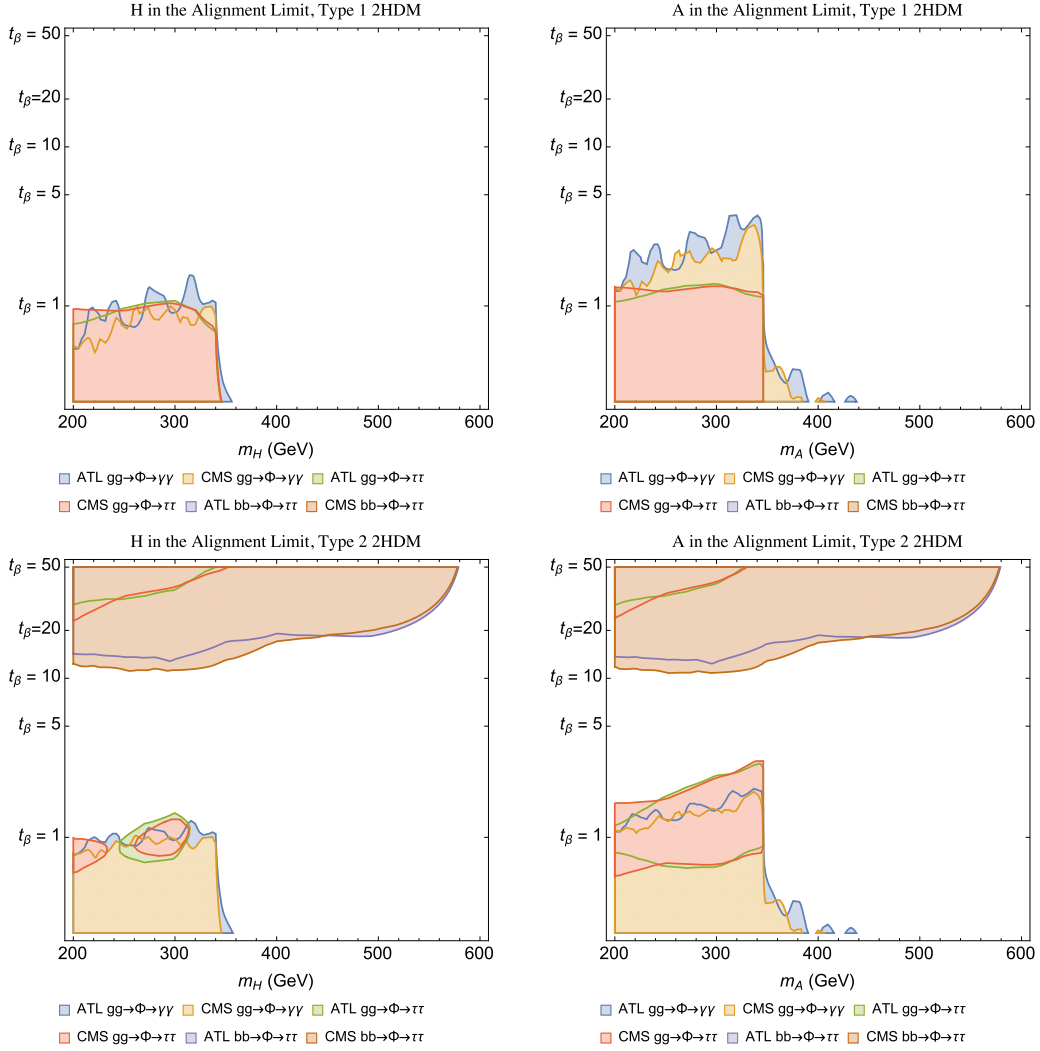


Figure 2: Top: Direct search limits on a heavy CP even neutral scalar H (left) and CP odd neutral pseudo-scalar A (right) as a function of mass in the alignment limit $\cos(\beta - \alpha) = 0$ in a Type 1 2HDM. Bottom: Same as above for a Type 2 2HDM.

As we move away from the exact alignment limit, vector boson associated production modes remain unimportant, but decays into vectors can become appreciable. Given the sensitivity of searches for heavy scalars decaying into SM bosons, searches in these final states become significant relatively close to the alignment limit. In figure 3 we present the state of direct searches for H/A with $m_{H/A} = 300$ GeV as a function of $\tan\beta$ and $\cos(\beta - \alpha)$ in Type 1 and Type 2 2HDM. As in the case of the exact alignment limit, for Type 1 2HDM sensitivity falls off with increasing $\tan\beta$ due to the falling production cross section. The strongest limits on H are provided by searches for gluon fusion production of H followed by decays into $ZZ \rightarrow 4\ell$, although these limits fall off near the alignment limit, where they

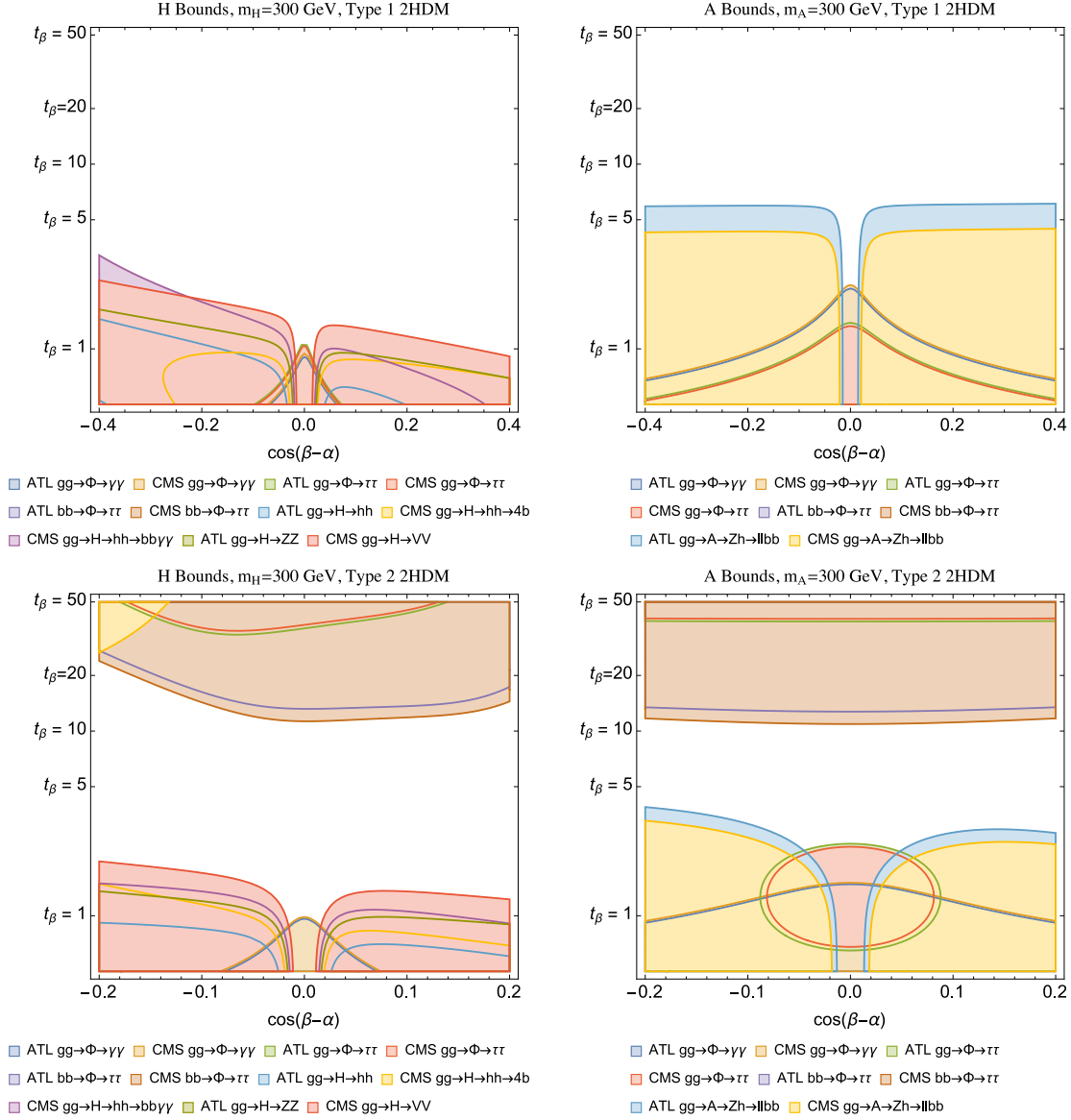


Figure 3: Top: Direct search limits on a 300 GeV CP even neutral scalar H (left) and CP odd neutral pseudo-scalar A (right) as a function of $\cos(\beta - \alpha)$ and $\tan\beta$ in a Type 1 2HDM. Bottom: Same as above for a Type 2 2HDM. Here we have taken $\lambda_{5,6,7} = 0$ in all plots. Note the different range of $\cos(\beta - \alpha)$ for Type 1 and Type 2 2HDM, motivated by the parameter space allowed by Higgs coupling fits.

are supplanted by searches for $H \rightarrow \gamma\gamma, \tau\tau$. The strongest limits on A come from searches for gluon fusion production of A followed by decay into $Zh \rightarrow \ell\ell b\bar{b}$. These limits likewise fall off near the alignment limit, where $A \rightarrow \gamma\gamma, \tau\tau$ provides complementary sensitivity. The situation for Type 2 2HDM is comparable to the Type 1 2HDM, save that searches in the

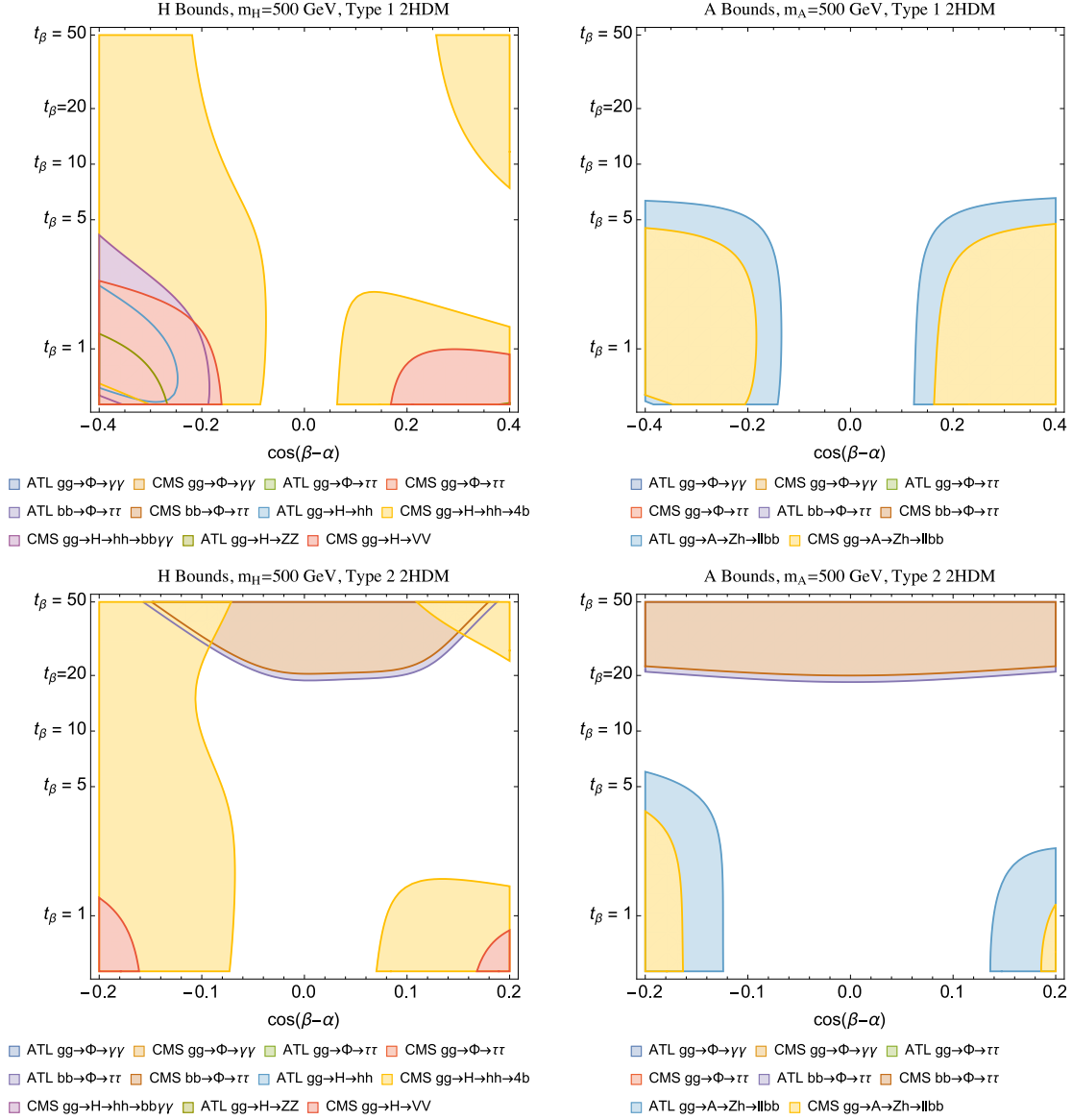


Figure 4: Top: Direct search limits on a 500 GeV CP even neutral scalar H (left) and CP odd neutral pseudo-scalar A (right) as a function of $\cos(\beta - \alpha)$ and $\tan \beta$ in a Type 1 2HDM. Bottom: Same as above for a Type 2 2HDM. Here we have taken $\lambda_{5,6,7} = 0$ in all plots. Note the different range of $\cos(\beta - \alpha)$ for Type 1 and Type 2 2HDM, motivated by the parameter space allowed by Higgs coupling fits.

$\tau\tau$ final state (either in gluon fusion or $b\bar{b}H/A$ associated production) become appreciable at large $\tan \beta$.

We repeat the process for heavier H/A in Type 1 and Type 2 2HDM with $m_{H/A} = 500$ GeV as a function of $\tan \beta$ and $\cos(\beta - \alpha)$ in figure 4. The limits are generally weaker compared

to $m_{H/A} = 300$ GeV, due both to falling signal cross sections and additional contributions to the total width from $H/A \rightarrow t\bar{t}$. However, notable exceptions are the bounds on $H \rightarrow hh$ from the CMS $H \rightarrow hh \rightarrow 4b$ search and the bounds on $A \rightarrow Zh$ from the ATLAS $A \rightarrow Zh \rightarrow \ell\ell b\bar{b}$ search. In particular, the considerable improvement in $H \rightarrow hh \rightarrow 4b$ sensitivity at high mass is due to the boosted kinematics of the $4b$ final state [51].

The combination of diverse searches for heavy Higgs bosons demonstrates considerable and complementary coverage across a wide range of 2HDM parameter space, but also highlights the substantial holes in existing coverage. In particular, in Type 1 2HDM, searches lose effectiveness at large $\tan\beta$ due to falling signal cross sections, and more generally lose sensitivity near the alignment limit when H/A can decay into $t\bar{t}$ pairs. In Type 2 2HDM there is additional sensitivity at large $\tan\beta$ due to enhanced gluon fusion and $b\bar{b}$ associated production, but sensitivity is poor at moderate $\tan\beta$. This is due to a combination of low production cross sections and, where kinematically available, missed decays into the $t\bar{t}$ final state. Among other things, these holes demonstrate the need for an effective $H/A \rightarrow t\bar{t}$ search.

3 Searching for a Neutral Higgs in $t\bar{t}$

As we have discussed, the natural place to look for new Higgs states heavier than about 350 GeV and with SM-like coupling strength to the top quark is in $gg \rightarrow H/A \rightarrow t\bar{t}$. It has been known since the seminal work of [39] (and recently emphasized in [37]) that this channel provides an interesting and challenging opportunity for hadron colliders. In contrast to searches for spin-1 or spin-2 $t\bar{t}$ resonances, the spin-0 signal amplitude interferes with the QCD background, producing a characteristic peak-dip structure. As such, existing searches for $t\bar{t}$ resonances cannot be meaningfully reinterpreted to place a constraint on additional Higgs bosons in the $t\bar{t}$ final state.

In this section we begin by revisiting the analysis of [39] with an eye towards the impact of detector effects in a realistic collider environment. Given the size of the SM $t\bar{t}$ background, we introduce a novel technique to efficiently model both detector and event reconstruction effects with adequate statistics. We find that because smearing of the reconstructed invariant mass of the $t\bar{t}$ system is typically the same order as (or larger than) the widths and range of interference effects of the new Higgs states, the peak-dip structure is largely washed out. While the statistical significance of the residual excess can become large at high luminosity, systematic effects are likely to render this channel unviable using standard reconstruction techniques.

We are thus motivated to consider ancillary probes of the $t\bar{t}$ final state that are not subject to the same interference effects, namely the associated production channels $t\bar{t}H/A \rightarrow t\bar{t}t\bar{t}$ and $b\bar{b}H/A \rightarrow b\bar{b}t\bar{t}$. We do not perform complete 14 TeV studies of these channels here, but we argue that – based on current 8 TeV trilepton limits – the four top quark channel in particular is likely to have sensitivity to moderate-mass scalars.

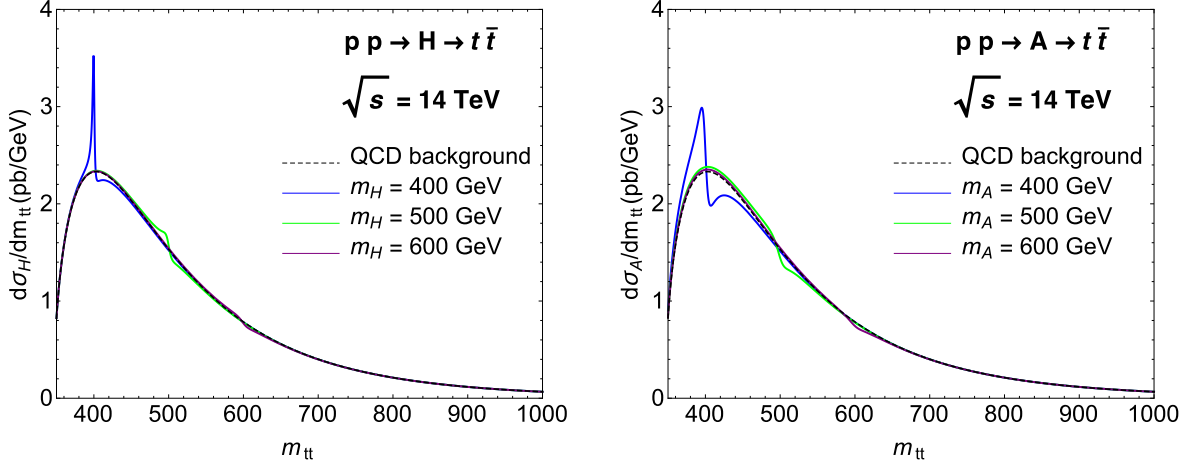


Figure 5: Cross sections vs $t\bar{t}$ invariant mass for $pp \rightarrow \Phi \rightarrow t\bar{t}$, where $\Phi = H$ (A) in the left (right) panel. The dashed black line shows the QCD background, and the different solid lines are associated to different values of the Φ mass.

3.1 $pp \rightarrow H/A \rightarrow t\bar{t}$

We begin by considering the leading-order interference effects between the $pp \rightarrow H/A \rightarrow t\bar{t}$ signal and the SM continuum $t\bar{t}$ background. In figure 5 we reproduce the differential rates for $pp \rightarrow H/A \rightarrow t\bar{t}$, combining the parton-level cross sections computed in [39] with the parton distribution functions (PDFs) evaluated in [54]. The coupling strengths are set by the SM top Yukawa and $m_t = 173$ GeV (the full $gg \rightarrow t\bar{t}$ differential cross section including all interference effects for general 2HDM couplings is given in appendix B). The characteristic peak-dip interference structure is apparent, particularly for heavier (pseudo)scalars; the signal-background interference term dominates the pure signal term for all heavy Higgs boson masses. This highlights the challenge facing searches for $H/A \rightarrow t\bar{t}$ at hadron colliders even before finite detector resolution is taken into account.

Given the size of the SM $t\bar{t}$ background and delicacy of the signal-background interference, it is crucial to incorporate detector effects with adequate Monte Carlo statistics. To efficiently simulate detector effects, we derive composite smearing functions for $t\bar{t}$ events as follows: We consider seven different reference values for the top quark pair invariant mass $m_{t\bar{t}}^0$, and for each we generate 10^6 QCD $t\bar{t}$ events in Madgraph [45], requiring $|m_{t\bar{t}} - m_{t\bar{t}}^0| < 0.5$ GeV. We then shower with PYTHIA6.4 [55] and process the events through Delphes3 [56, 57]. We then reconstruct the semi-leptonic $t\bar{t}$ system using mass-shell constraints as detailed in appendix C, thereby obtaining a response function mapping $m_{t\bar{t}}^0$ to an $m_{t\bar{t}}$ distribution. In figure 6 we plot histograms of these $m_{t\bar{t}}$ distributions. Interpolating numerically in $m_{t\bar{t}}^0$ and $m_{t\bar{t}}$, we obtain a kernel $P(m_{t\bar{t}}^0, m_{t\bar{t}})$ against which we can convolve the PDF-smearred parton-level differential cross section. This allows us to model the effects of detector resolution and $t\bar{t}$ reconstruction on the peak-dip structure without being limited by Monte Carlo statistics. We plot the results

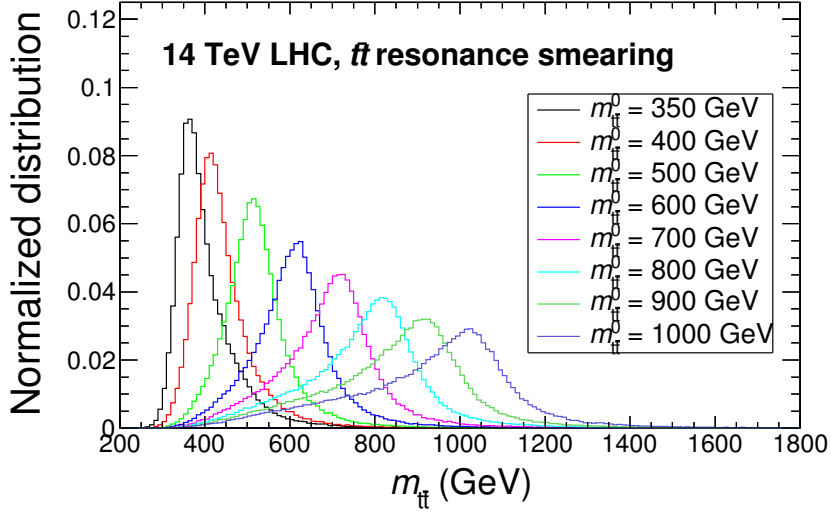


Figure 6: Distribution of $m_{t\bar{t}}$ after detector effects and $t\bar{t}$ reconstruction for different values of the produced top quark pair mass $m_{t\bar{t}}^0$.

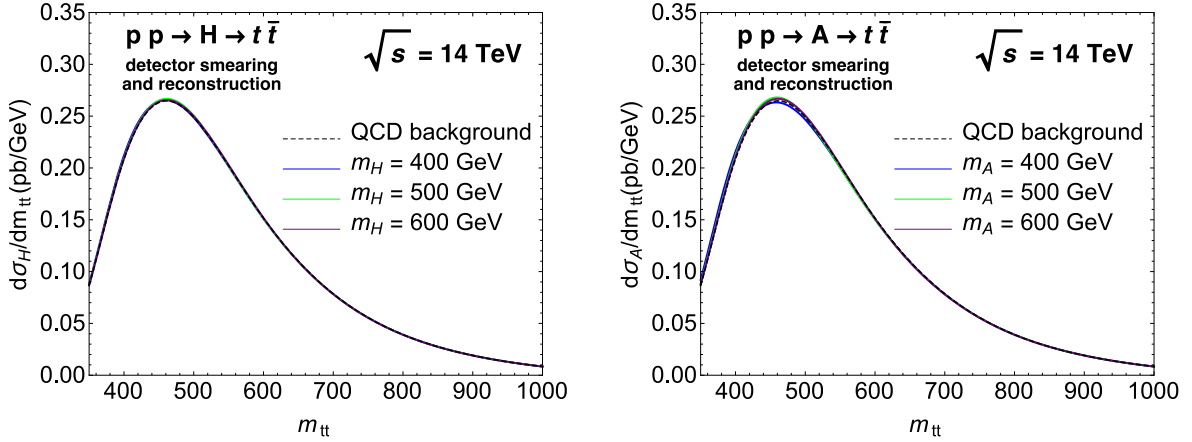


Figure 7: Cross sections vs $t\bar{t}$ invariant mass for $pp \rightarrow \Phi \rightarrow t\bar{t}$, where $\Phi = H$ (A) in the left (right) panel. Relative to figure 6, we now include detector and reconstruction effects. In figure 8 we plot the difference between the background and signal+background curves.

in the two panels of figure 7 for the scalar and the pseudoscalar.

Detector resolution and $t\bar{t}$ reconstruction completely erode the peak-dip structure in the presence of a heavy Higgs, leaving behind only modest shifts in the $t\bar{t}$ invariant mass distribution relative to the QCD prediction. In figure 8 we plot the difference between the smeared invariant mass spectra predicted by QCD with a heavy Higgs boson and pure QCD. The best- $m_{t\bar{t}}$ -bin statistical significances $\sqrt{\Delta\chi^2}$ at 3000 fb^{-1} and the corresponding S/B are

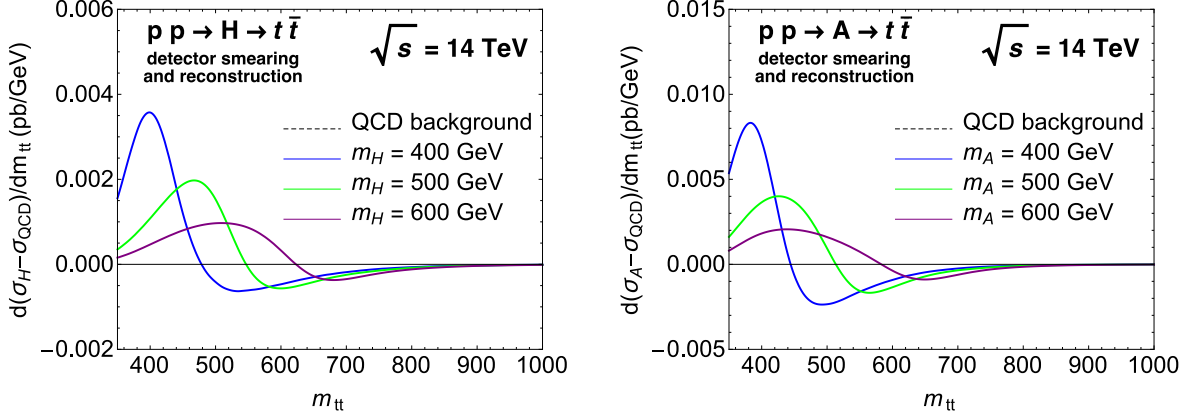


Figure 8: Difference between the background-only and signal+background cross section curves shown in figure 7 for $pp \rightarrow \Phi \rightarrow t\bar{t}$, where $\Phi = H$ (A) in the left (right) panel.

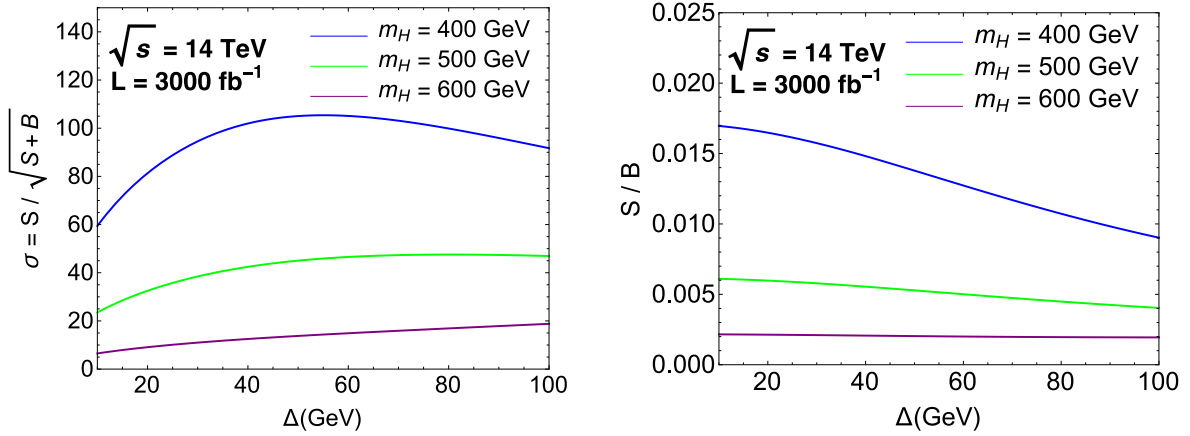


Figure 9: Left: Best- $m_{t\bar{t}}$ -bin statistical significance expected at 3000 fb^{-1} for the scalar case as a function of bin width Δ . Right: the corresponding S/B . Qualitatively similar results hold for the pseudoscalar resonance.

shown for the scalar resonance in figure 9 as a function of bin size; qualitatively similar results hold for the pseudoscalar. From these figures, we conclude that although the high-luminosity LHC will have sufficient statistical power to observe $H/A \rightarrow t\bar{t}$ in principle, systematic uncertainties (even at the percent level) will almost certainly prevent any significant detection. Although we have only considered signal and background and leading order (as full next-to-leading-order (NLO) expressions for signal+background do not yet exist), it is unlikely that the inclusion of NLO effects will significantly alter these conclusions.

Of course, there is more information in the $t\bar{t}$ final state than just the invariant mass; angular distributions and spin correlations may provide additional handles. In appendix B we present a parametrization of the $t\bar{t}$ differential cross section in terms of a well behaved scat-

tering variable that affords some additional discrimination between signal and background. A full multivariate analysis employing all this ancillary information would increase the sensitivity incrementally, but we do not expect this would substantially alter our conclusions.

3.2 $pp \rightarrow b\bar{b}H/A \rightarrow b\bar{b}t\bar{t}$ and $pp \rightarrow t\bar{t}H/A \rightarrow t\bar{t}t\bar{t}$

Given the considerable challenges facing a search in the $t\bar{t}$ final state, it is useful to consider associated production modes in conjunction with $H/A \rightarrow t\bar{t}$. In the alignment limit, vector associated production modes for H such as Higgs strahlung or VBF are strongly suppressed, while such modes are entirely nonexistent for A . This suggests focusing on fermionic associated production modes such as $t\bar{t}H/A$ or $b\bar{b}H/A$. The former is appreciable at low $\tan\beta$ in both 2HDM types, while the latter is appreciable at moderate to large $\tan\beta$ in Type 2 2HDM such as the Minimal Supersymmetric Standard Model (MSSM).

Let us first consider $t\bar{t}$ associated production of H or A followed by decay to $t\bar{t}$. On one hand, the resulting 4-top final state provides an abundance of promising signal channels. On the other hand, the massive three-body kinematics of $t\bar{t}$ associated production with $m_{H/A} \gtrsim 2m_t$ lead to at most a $\mathcal{O}(\text{fb})$ rate at 8 TeV. Prospects improve significantly at $\sqrt{s} = 14$ TeV, but even here the production cross section is at most in the tens of femtobarn.

There are a variety of searches at $\sqrt{s} = 8$ TeV that are sensitive to the 4-top final state, particularly those involving same-sign dileptons (SSDL) or multileptons with additional b -tagged jets. To estimate the reach of the 4 top channel at $\sqrt{s} = 8$ TeV, we reinterpret an 8 TeV CMS multilepton search [58]. We use SRs 8, 18, and 28 of [58]. These signal regions are all characterized by trilepton events with a Z -veto, at least four jets with two b -tags, and $H_T > 200$ GeV, and are distinguished by \cancel{E}_T in the range 50-100 GeV, 100-200 GeV, and ≥ 200 GeV, respectively. We compute the acceptance times efficiency for $t\bar{t}H/A \rightarrow t\bar{t}t\bar{t}$ signals in these signal regions using Madgraph/Pythia/Delphes as above. Signal regions 8 and 18 are the most sensitive, with SR 28 contributing additional sensitivity for larger values of $m_{H/A}$. To set limits using the observed event counts in [58], we treat each bin as an independent Poisson variable and combine limits from individual bins using a Bayesian algorithm with a flat prior on signal strength, marginalizing over a normally-distributed background uncertainty. We neglect potential uncertainties on the signal cross section.

The 8 TeV data is insufficient to set a limit on a SM-like $Ht\bar{t}$ coupling. For example, we find for $m_H = 350$ GeV that the combination of SRs 8, 18, 28 exclude $\sigma \cdot \text{Br} \gtrsim 160$ fb. By contrast, for $m_H = 350$ GeV and $\tan\beta = 1$ we have $\sigma(pp \rightarrow t\bar{t}H) \simeq 5$ fb at $\sqrt{s} = 8$ TeV, placing the signal cross section more than an order of magnitude below the current exclusion in this channel. While the inclusion of additional channels such as SSDL would improve sensitivity, the disparity between signal cross section and exclusion too great to hope for meaningful sensitivity in this channel at $\sqrt{s} = 8$ TeV. Although we have explicitly considered the case of $pp \rightarrow t\bar{t}H$, the rate for $pp \rightarrow t\bar{t}A$ is comparable, and degenerate H/A in the alignment limit would lead to a doubling of the signal.

At $\sqrt{s} = 14$ TeV the prospects for a search in the 4-top channel improve considerably, as the $t\bar{t}H/A$ associated production cross section increases by an order of magnitude for

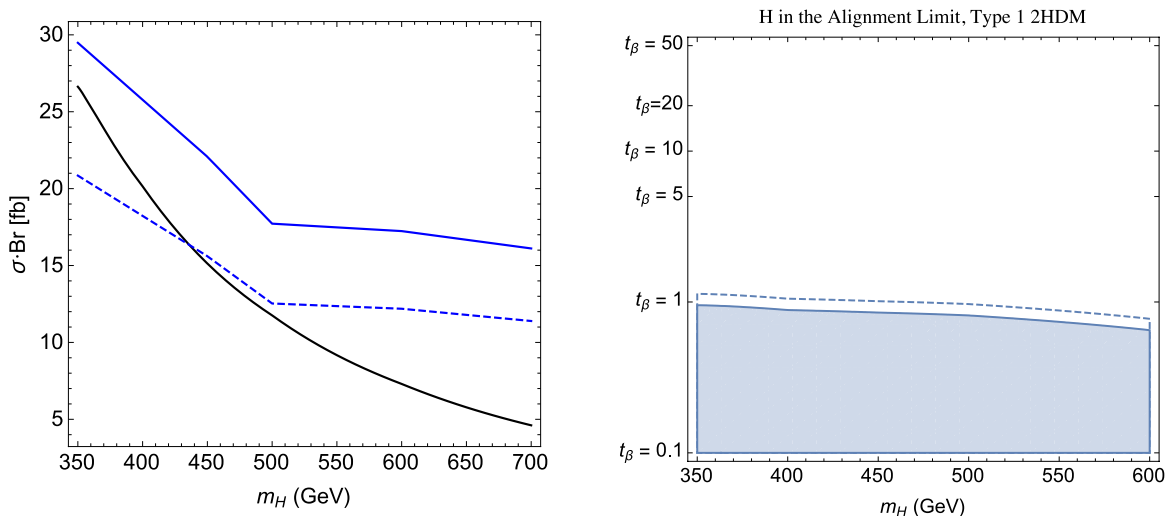


Figure 10: Left: Projection for the excluded cross section times branching ratio for $pp \rightarrow t\bar{t}H \rightarrow t\bar{t}t\bar{t}$ at $\sqrt{s} = 14$ TeV, 3000 fb^{-1} as a function of m_H . The projection is obtained from the naive scaling of the combination of $3\ell + 2b$ channels (solid blue line) and with a further $\sqrt{2}$ improvement from the addition of SSDL channels (dashed blue line), and is compared to the signal cross section $\sigma(pp \rightarrow t\bar{t}H)$ at $\tan\beta = 1$ (solid black line). Right: Projected exclusion for a CP-even neutral scalar H in the alignment limit of a Type 1 2HDM from the naive scaling of the combination of $3\ell + 2b$ channels (solid blue) and with a further $\sqrt{2}$ improvement from the addition of SSDL channels (dashed blue).

$m_{H/A} \gtrsim 2m_t$ relative to $\sqrt{s} = 8$ TeV. However, reliably estimating sensitivity at the level of a theory study is challenging since the largest backgrounds to SSDL and multi-lepton searches in this final state typically originate from $t\bar{t}$ or $W/Z + \text{jets}$ events with an additional fake lepton. As such, we estimate the 14 TeV $\sigma \times \text{Br}$ exclusion reach with luminosity and background cross section rescaling of [58], assuming efficiencies remain comparable to 8 TeV. In particular, we rescale background cross sections by the ratio of $t\bar{t}$ cross sections at 14 TeV and 8 TeV, since $t\bar{t} + \text{lepton fakes}$ comprise the dominant background in signal regions 8, 18, and 28 of [58].

The impact of this projected sensitivity at $\sqrt{s} = 14$ TeV is shown in figure 10, both for the naive scaling of the sensitivity from the combination of $3\ell + 2b$ channels, and with an additional factor-of- $\sqrt{2}$ improvement in the $\sigma \cdot \text{Br}$ reach to emulate the potential improvement from including SSDL channels. Even at $\sqrt{s} = 14$ TeV this remains a challenging channel, but offers hope for meaningful sensitivity at low $\tan\beta$ for $2m_t \lesssim m_H \lesssim 500$ GeV.

We turn next to $b\bar{b}$ associated production of H or A followed by decay to $t\bar{t}$. This process may be significant in Type 2 2HDM where the $b\bar{b}H/A$ associated production grows with $\tan\beta$. However, in this case the partial width $H/A \rightarrow t\bar{t}$ also falls as with $\tan\beta$, suggesting the rate for $b\bar{b}H/A \rightarrow b\bar{b}t\bar{t}$ will peak at moderate values of $\tan\beta$. To estimate the LHC

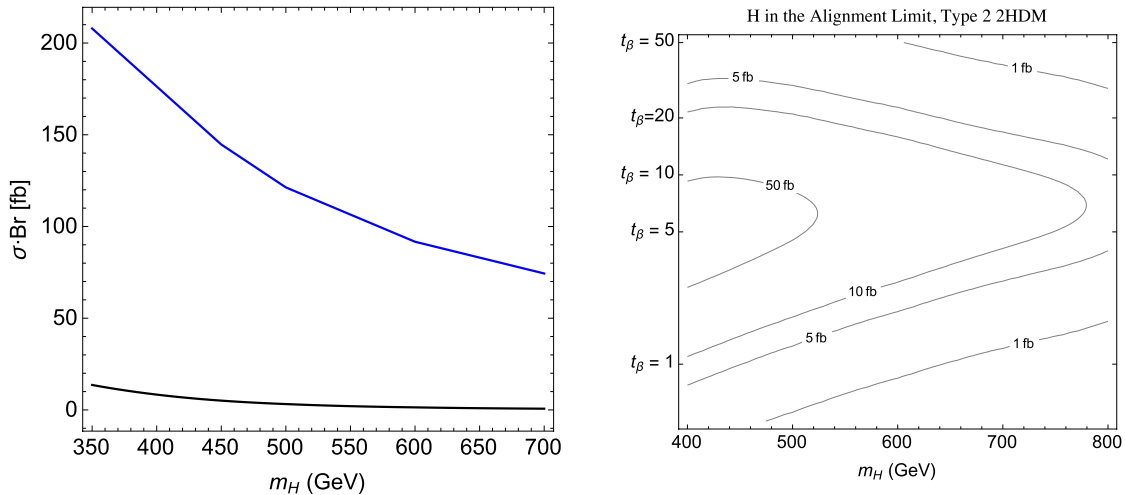


Figure 11: Left: Projection for the excluded cross section times branching ratio in femtobarns for $pp \rightarrow b\bar{b}H \rightarrow b\bar{b}t\bar{t}$ at $\sqrt{s} = 14$ TeV, 3000 fb^{-1} as a function of m_H (solid blue line). For comparison we show the signal cross section $\sigma(pp \rightarrow b\bar{b}H)$ at $\tan\beta = 1$ (solid black line). Right: Contours of $\sigma \cdot \text{Br}(pp \rightarrow b\bar{b}H \rightarrow b\bar{b}t\bar{t})$ in femtobarns for a CP-even neutral scalar H in the alignment limit of a Type 2 2HDM.

sensitivity to $pp \rightarrow b\bar{b}H/A \rightarrow b\bar{b}t\bar{t}$, we design and simulate a search in the semi-leptonic final state at $\sqrt{s} = 14$ TeV. In contrast to the multi-lepton search for the four-top final state, the dominant backgrounds for a $t\bar{t}b\bar{b}$ final state can be reliably simulated with available Monte Carlo techniques.

We generate parton level signal and background events using MadGraph5 [45] to leading order with CTEQ6L1 PDFs [59]. The events are showered with PYTHIA6.4 [55] and Delphes3 [56, 57] is used to simulate detector effects. Jets are reconstructed using the anti- k_T algorithm with $R = 0.5$ and are required to satisfy $p_T^j > 20 \text{ GeV}$, $|\eta^j| < 4.5$. Charged leptons (electrons and muons) are required to have $p_T^\ell > 15 \text{ GeV}$, $|\eta^\ell| < 2.5$, $I_{iso,\mu}(\Delta R = 0.3) < 0.1$. The b -tagging efficiency is chosen to be 70% with a 25% (2%) mistagging rate for charm (light) jets [60]. b -tagged jets satisfy $p_T^b > 40 \text{ GeV}$, $|\eta^j| < 2.5$.

In addition to the single lepton requirement, we require at least 6 jets with at least 4 b -tags in the final state to suppress SM backgrounds. We also apply a missing transverse energy cut of $\cancel{E}_T > 30 \text{ GeV}$ and veto events with more than one charged lepton. Top quarks and W bosons are reconstructed from the mass-shell constraints, with small corrections for detector effects (for details, see appendix C). After top quark reconstruction, we require that the signal events satisfy $\chi^2 < 5.0$, where χ is a variable characterizing the quality of the reconstruction (see appendix C). The irreducible background is $pp \rightarrow t\bar{t}b\bar{b}$, while the dominant reducible backgrounds for this analysis are $pp \rightarrow t\bar{t}bj$ and $pp \rightarrow t\bar{t}jj$, with light jets faking bottom quarks. The backgrounds from $t\bar{t}h$, $t\bar{t}Z$, single top production and vector boson plus

multijets are subdominant [61].

To set an exclusion limit, we use the likelihood function

$$L(x|n) = \prod_{j=1}^N \frac{x_j^{n_j}}{n_j!} e^{-x_j}, \quad (3.1)$$

where x_j is the binned $m_{t\bar{t}}$ distribution predicted by the model (with or without signal) and n_j is the observed distribution. The 2σ exclusion bound is obtained [62] from

$$\sqrt{-2 \ln \left(\frac{L(\mu s + b|b)}{L(b|b)} \right)} = 2. \quad (3.2)$$

The results are shown in figure 11. The excluded cross section ranges from 200-70 fb for $350 \text{ GeV} \lesssim m_H \lesssim 700 \text{ GeV}$, while $\sigma(pp \rightarrow b\bar{b}H) \lesssim 10 \text{ fb}$ for $\tan\beta = 1$ across the same range. Although the production cross section grows with $\tan\beta$, the branching ratio to $t\bar{t}$ falls, so that the peak rate $\sigma(pp \rightarrow b\bar{b}H \rightarrow b\bar{b}t\bar{t}) \sim 50 \text{ fb}$ is obtained around $\tan\beta \sim 5$. Based on the results of our preliminary simulation, a meaningful limit cannot be set in Type 2 2HDM. However, given that sensitivity is of the same order as the peak rate for $350 \text{ GeV} \lesssim m_H \lesssim 500 \text{ GeV}$, this channel deserves further experimental study at 14 TeV.

Finally, we note a third associated production channel that may prove useful in the hunt for $H/A \rightarrow t\bar{t}$, although we do not study it in detail here. The rate for electroweak production of the single-top $t(q)H/A$ final state via a t -channel W boson exceeds that of $t\bar{t}H/A$ production around $m_{H/A} \simeq 340 \text{ GeV}$ [63] and has the same parametric scaling as a function of α and β . Consequently, this suggests the rate for $pp \rightarrow t(q)H/A \rightarrow t(q)t\bar{t}$ exceeds that of $pp \rightarrow t\bar{t}H/A \rightarrow t\bar{t}t\bar{t}$ in the entire region of interest for $H/A \rightarrow t\bar{t}$. The resulting three-top final state is particularly amenable to a search for same-sign dileptons with two or more b -tagged jets, and may provide a complementary probe of $H/A \rightarrow t\bar{t}$ at $\sqrt{s} = 14 \text{ TeV}$.⁴

4 Searching for an Invisible Neutral Higgs

In addition to decays of new scalars to SM fermions, it is also interesting to consider invisible decays, which have been actively studied for the SM Higgs boson following Run 1 (with current upper limits around 30% coming from the VBF channel [65]). As with the SM Higgs, any observation of an invisible width for a second Higgs state would provide a window into new physics, possibly signaling the first laboratory production of dark matter. Invisible decays could also provide a discovery mode for new Higgses, since SM backgrounds can be strongly suppressed with a large missing energy cut. In this section, we continue the study of new scalars in channels involving tops and bottoms, adding the ingredient of large missing energy.

In section 4.1 we briefly discuss some of the theoretical motivation for searching for invisibly decaying new scalars in association with tops and bottoms. There are many possible

⁴For a recent study of single top production in association with the Higgs state at 125 GeV, see [64].

UV completions. For simplicity we focus on one amusing example, the MSSM Higgs sector benchmark points often used in reporting limits on $H/A \rightarrow \tau\tau$. Due to choice of neutralino mass parameters in these benchmark points, the new neutral scalars associated with the second Higgs doublet possess branching fractions into pairs of the lightest R -odd particle. With some variation of the parameters, the invisible branchings can become substantial.

In section 4.2, we place a limit on $b\bar{b}H \rightarrow b\bar{b} + \cancel{E}_T$ by reinterpreting an 8 TeV sbottom search [66]. We give the corresponding limit in the parameter space of Type 2 2HDM, where the $b\bar{b}H$ coupling is $\tan\beta$ -enhanced, and argue that it is likely to be a stronger limit on this parameter space than one derived from monojet searches. Previously, in a study focused on dark matter simplified models, Ref. [67] obtained a limit on the $b\bar{b}$ -associated invisible scalar channel by reinterpreting an ATLAS effective operator study at 8 TeV [68]. We have checked that the sbottom and effective operator cut flows provide very similar reach, and present our results on natural parameter spaces for new scalar searches.

In section 4.3 we study the reach of semileptonic $t\bar{t}H \rightarrow t\bar{t} + \cancel{E}_T$ at 14 TeV. Previously, Ref. [69] obtained a limit on this channel at 8 TeV by reinterpreting a CMS stop search [70]. Ref. [71] also performed an 8 TeV analysis, and furthermore estimated a 14 TeV limit by a parton-level reinterpretation of an ATLAS stop study [72]. We complete the phenomenological analysis of semileptonic $t\bar{t}H \rightarrow t\bar{t} + \cancel{E}_T$, performing a full 14 TeV analysis with optimized cuts and detector simulation. We also argue that this channel is likely to be competitive with monojet searches for new invisibly-decaying scalars with masses below $2m_t$.

4.1 Models with $H/A \rightarrow \cancel{E}_T$

In the most model-independent spirit of simplified models, any search for an invisibly decaying new scalar is of interest: the topologies are simple and capitalize on the small SM backgrounds. The production channels studied here are motivated by the alignment limits of new weakly-coupled scalar models, which preserve the SM-like properties of the light observed Higgs boson at the expense of suppressing traditional invisible scalar searches involving gauge couplings such as $ZH \rightarrow \ell\ell + \cancel{E}_T$ and $qqH \rightarrow qq + \cancel{E}_T$. It is not difficult to add additional theoretical structure, such as dark matter candidates or particles that are long-lived on detector timescales, into which new scalar states may decay invisibly with substantial branching fraction.

Searches in the $t\bar{t} + \cancel{E}_T$ channel are most effective in models where new scalars couple to $t\bar{t}$ with coupling $y'_t \sim y_t^{\text{SM}}$. In the alignment limits of Type 1 and Type 2 2HDM, $y'_t/y_t^{\text{SM}} = \cos\beta$ and $y'_t/y_t^{\text{SM}} = \cot\beta$, respectively, so the LHC reach is strongest when $\tan\beta \sim \mathcal{O}(1)$. A simple model of invisible decays can be obtained by coupling the second doublet Φ_2 to a new massive singlet scalar through a portal-type coupling:

$$V \supset \kappa |\Phi_2|^2 S^2 + \frac{1}{2} \mu_s^2 S^2 + \dots \quad (4.1)$$

In the alignment limit, the dominant decays of the neutral components H, A of Φ_2 will be into Standard Model fermions and S pairs. Let us assume that the singlet mass is small and

that $m_H \lesssim 2m_t$, so that the dominant SM decays are into $b\bar{b}$. Then the ratio of invisible to visible partial widths is approximately:

$$\frac{\Gamma_{SS}}{\Gamma_{b\bar{b}}} \simeq \frac{\kappa^2 v^2 \cos^2 \beta}{3m_H^2 y_b'^2}. \quad (4.2)$$

In Type 1 2HDM, $y_b' = y_b^{\text{SM}} \cos \beta$ in the alignment limit, so this ratio is $\mathcal{O}(1)$ already for $\kappa \sim 0.1$ in the range of m_H considered. In Type 2 2HDM, y_b' is $\tan \beta$ -enhanced in the alignment limit, but for $\tan \beta \sim \mathcal{O}(1)$ the invisible decay is still substantial for small κ . Simple models of this type are most effectively probed by the $t\bar{t} + \cancel{E}_T$ channel.

Since y_b^{SM} is small, searches for $b\bar{b} + \cancel{E}_T$ are most effective in cases where the new scalar has enhanced coupling y_b' to $b\bar{b}$. The most well-known example is the $\tan \beta$ enhancement of the Type 2 2HDM. In the toy model above, the ratio of partial widths is suppressed by $(\tan \beta)^{-4}$, so κ must be large in order to obtain a substantial invisible width. Another Type 2 2HDM with the potential for invisible decays is the MSSM. In fact, traditional benchmark scenarios used to study $H/A \rightarrow \tau\tau$ actually have regions of parameter space where $H/A \rightarrow \text{inv}$ occurs at non-negligible rates [73].

Supersymmetric Higgs bosons couple to neutralinos in the form Higgs - Higgsino - Electroweakino. Therefore, for $\mu \sim M_i \ll m_A$ ($i = 1$ or 2), the heavy neutral Higgs states can decay invisibly into the lightest neutralino through its gaugino/higgsino mixings. The invisible branching ratios for H are maximized for $\tan \beta \sim 5$; at higher values $H \rightarrow b\bar{b}$ dominates, while at lower values we deviate substantially from the alignment limit and $H \rightarrow VV$ becomes important. In figure 16 we show the $H/A \rightarrow \text{inv}$ branching ratios in an MSSM benchmark point with $\tan \beta = 5$, $M_2 = 300$ GeV, $M_1 = (5s_w^2/3c_w^2)M_2 = 143$ GeV, and decoupled gluino and scalars. Sizable invisible branching fractions are possible for both states when the LSP is well-mixed and the $t\bar{t}$ channel is kinematically forbidden.

We do not pursue model building further in this work, but for completeness we note that LUX limits [74] rule out most of the interesting parameter space if the neutralino is dark matter and $\mu > 0$. If it is only a subcomponent of dark matter, or if it is stable on detector timescales but decays outside of the detector (say, through RPV couplings, or to a gravitino), then the direct detection limits do not apply. Another intriguing possibility is that $\mu < 0$. Ref. [75] observed that for $|\mu| \sim m_{\text{LSP}}$, and $\tan \beta \sim \text{few}$, there is a blind spot on the m_H axis where the tree-level direct detection amplitudes from SM Higgs and MSSM Higgs exchange cancel with each other.

4.2 $b\bar{b} + \cancel{E}_T$ at 8 TeV

In this section, we reinterpret the ATLAS sbottom search ($pp \rightarrow b\bar{b} + \cancel{E}_T$) performed in Ref. [66] into a limit on $pp \rightarrow Hb\bar{b}$, where H is a new heavy neutral CP-even scalar that decays invisibly. We unfold the signal efficiency factors from the cross section limits σ_{vis} given in Table 7 of [66]. We focus on Signal Region A (SRA), defined by the cut flow of Table 1 of [66], because in that region the leading two jets are b-tagged. SRA is divided into five

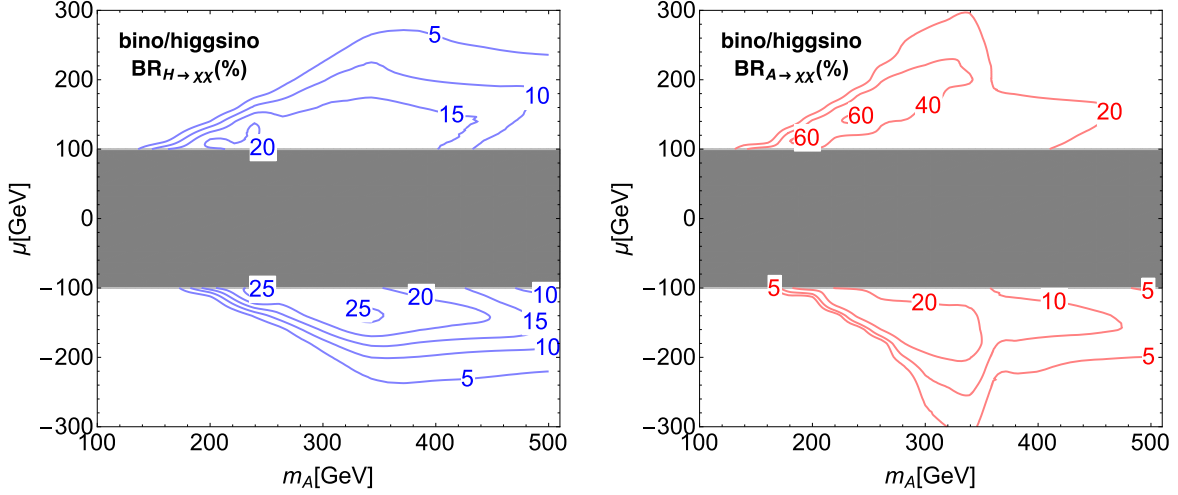


Figure 12: Contours of the $H/A \rightarrow \text{inv}$ branching ratios in an MSSM benchmark point with $\tan \beta = 5$, $M_2 = 300$ GeV, $M_1 = (5s_w^2/3c_w^2)M_2 = 143$ GeV, and decoupled gluino and scalars. The gray region denotes the LEP exclusion on light charginos.

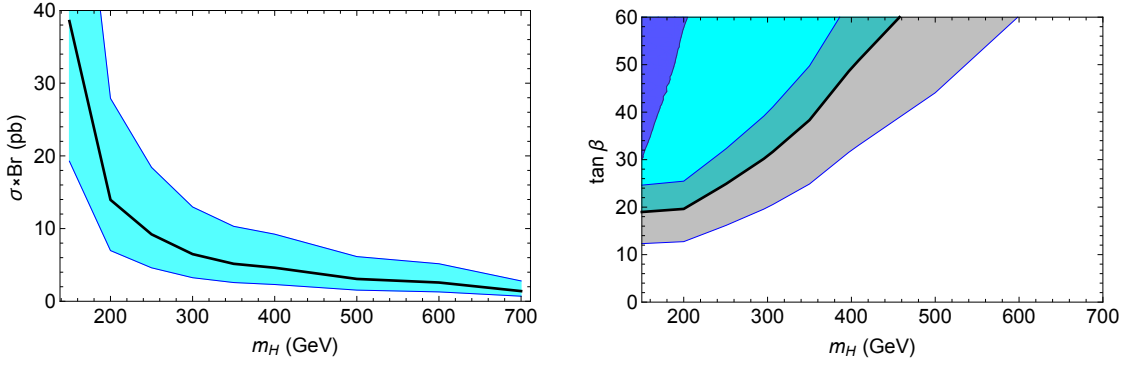


Figure 13: Left: the 8 TeV $\sigma \times \text{Br}$ limit on the production of invisibly decaying new scalars in association with bottom quarks. Right: the corresponding limit on the Type 2 2HDM plane. The lighter blue region in the upper left is the $b\bar{b} + \cancel{E}_T$ exclusion and the darker blue region is the estimated monojet exclusion, rescaling the results of [76].

subregions based on the contranverse mass cut [77] (with ISR correction given in [78]), and the ATLAS observed limits on the cross sections in SRA range from $0.26 - 1.9$ fb depending on the m_{CT} cut.

For signal generation and detector simulation we use Madgraph/Pythia/Delphes matched to one jet. We optimize the unfolded $\sigma_{pp \rightarrow b\bar{b}H} \times \text{Br}(H \rightarrow \text{inv})$ over the m_{CT} cut, finding that the softest cut used in the sbottom search ($m_{CT} > 150$ GeV) gives the best limit on bbH until $m_H \gtrsim 600$ GeV. We attempt to validate our analysis by reproducing the sbottom signal efficiencies given in the ancillary data of [66]. We find that near the exclusion limit

our analysis yields signal efficiencies approximately a factor of 2 better than those found by ATLAS. Therefore, to be conservative we assign a factor of $(1/2, 2)$ uncertainty band to our bbH limit.

Our results for the $\sigma \times \text{Br}$ limit are given in the left-hand panel of figure 13. The cross sections are relatively large, suggesting that this search mode is most effective in constraining new scalar models where the scalar coupling to bottom quarks is enhanced over that of the SM Higgs. Such enhancements occur, for example, in the alignment limit of Type 2 2HDM, where at large $\tan\beta$ the Hbb and Abb couplings are a factor of $\tan\beta$ larger than the SM Higgs hbb coupling. In the right-hand panel of figure 13, we reinterpret the $\sigma \times \text{Br}$ limit on the parameter space of Type 2 models with $\text{Br}(H \rightarrow \text{inv}) = 1$.

We note that a monojet signal arises in this scenario by closing the bottom loop and radiating an additional jet. In the case of $t\bar{t} + \cancel{E}_T$, the monojet signature obtained in this way is competitive and can outperform reinterpreted stop searches [71]. However, in the $b\bar{b} + \cancel{E}_T$ case, we expect that monojet is less powerful for two reasons. First, unlike the $t\bar{t} + \cancel{E}_T$ case, the bottom quarks in the final state do not suffer a large phase-space suppression. Second, closing the loop costs a factor of m_f in the amplitude, which is a large suppression in the $b\bar{b}$ case, even if the coupling to bottom quarks is $\tan\beta$ -enhanced. (Moreover, in some models, like Type 2 2HDM, the new scalar coupling to top quarks is $\tan\beta$ -suppressed.) In the dark blue region of the right-hand panel of figure 13 we estimate the monojet exclusion by rescaling the results of [76] into the Type 2 plane, and we see that it is much weaker than $b\bar{b} + \cancel{E}_T$. Our rescaling uses the ratio of the LO $\Gamma(H \rightarrow gg)$ loop functions in the 2HDM relative to the SM, and is therefore rather crude. However, it is likely to be conservative, since the p_T spectrum of the extra jet in the bottom-dominated process is harder than that of the jet in the top-dominated case [79], suggesting that the actual monojet limits will be weaker.

4.3 $t\bar{t} + \cancel{E}_T$ at 14 TeV

We now turn to invisible Higgs states produced in association with top quarks, where limits at 8 TeV have been obtained [69, 71] by reinterpretation of a CMS stop search [70], and perform an optimized projection for the reach of the 14 TeV LHC. We simulate signal and background at leading order in Madgraph/Pythia/Delphes, and apply cuts requiring large missing energy, four jets including two b -tags, and a veto on $n_{lep} \neq 1$. The dominant SM background processes are semileptonic and dileptonic $t\bar{t}$, $Zt\bar{t} \rightarrow \nu\nu\ell\nu jjb\bar{b}$, and $Wjjb\bar{b}$.

For our preselection and jet selection cuts, we require $\cancel{E}_T > 250$ GeV, 1 lepton, at least four central jets with $p_T > \{130, 50, 50, 30\}$, respectively, two b -tags, and $\Delta\phi(j, \cancel{E}_T) > 0.8$ for the two hardest jets. In stop searches, hard cuts on the transverse mass m_T and the variable $m_{T_2}^W$ [80] may be used to suppress semileptonic and dileptonic $t\bar{t}$, respectively [70]. The distributions of \cancel{E}_T , m_T , and $m_{T_2}^W$ after the jet selection cuts are given in Figs. 14, 15, and 16 for backgrounds and signal for two values of the scalar mass. Subsequently we optimize cuts on \cancel{E}_T , m_T , and $m_{T_2}^W$, choosing $\cancel{E}_T > 300$ GeV, $m_T > 140$ GeV, and $m_{T_2}^W > 200$ GeV. After all cuts, $Zt\bar{t}$ is the dominant background. Subsequently we validate the $Zt\bar{t}$ backgrounds against the stop search study in Ref. [70].

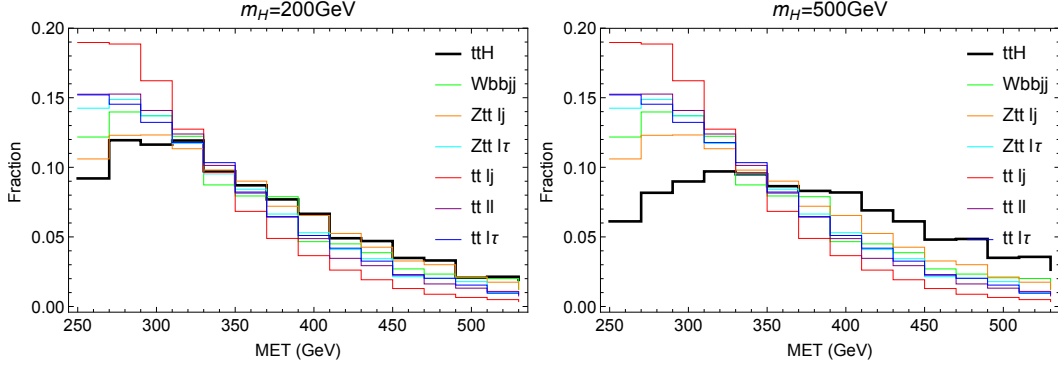


Figure 14: The \cancel{E}_T distributions of the signal and backgrounds after the jet selection cuts described in the text. Left: $m_H = 200$ GeV. Right: $m_H = 500$ GeV.

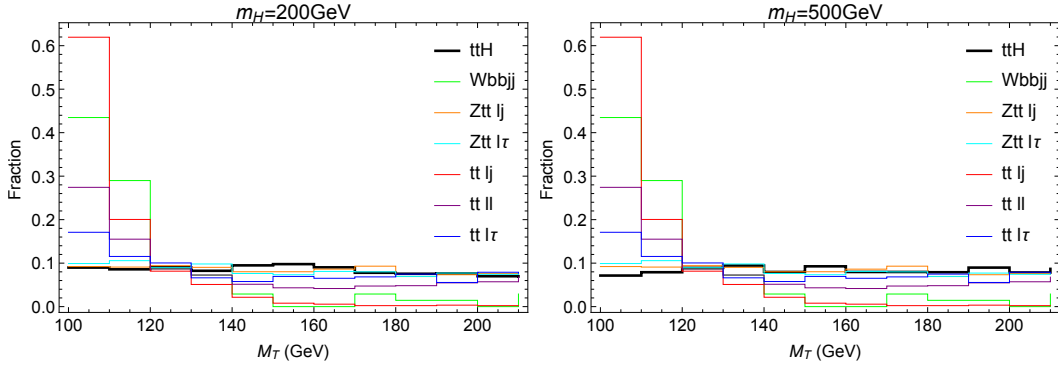


Figure 15: The m_T distributions of the signal and backgrounds after the jet selection cuts described in the text. Left: $m_H = 200$ GeV. Right: $m_H = 500$ GeV.

Our projected limit ($CL_s = 0.05$) with 300fb^{-1} is given in the left-hand panel of figure 17. It is also interesting to compare with the monojet reach, which we take from the scalar analysis performed in [76]. Unlike in the $b\bar{b} + \cancel{E}_T$ case, the $t\bar{t} + \cancel{E}_T$ search is most effective when the new states have SM-like couplings to top quarks. Therefore, rather than comparing the reaches in the parameter space of a Type 2 2HDM, we compare the reaches relative to a SM-like fiducial model with a new scalar decaying invisibly with unit branching ratio. (Of course, above the $t\bar{t}$ threshold, such a large invisible branching ratio would require a very large coupling to the invisible states; the fiducial model is meant only for the comparison of the two search modes.) The right-hand panel of figure 17 shows that the associated production mode is expected to be competitive with monojet limit until around the $t\bar{t}$ threshold, where the threshold generates a bump in the SM monojet cross section.

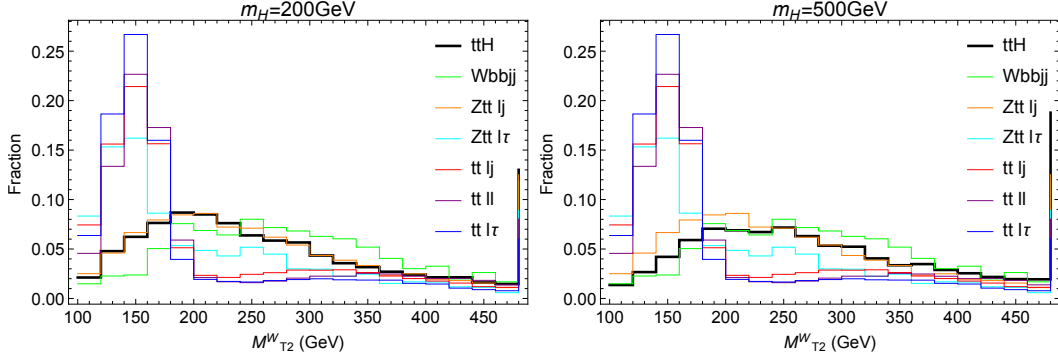


Figure 16: The $m_{T_2}^W$ distributions of the signal and backgrounds after the jet selection cuts described in the text. Left: $m_H = 200$ GeV. Right: $m_H = 500$ GeV.

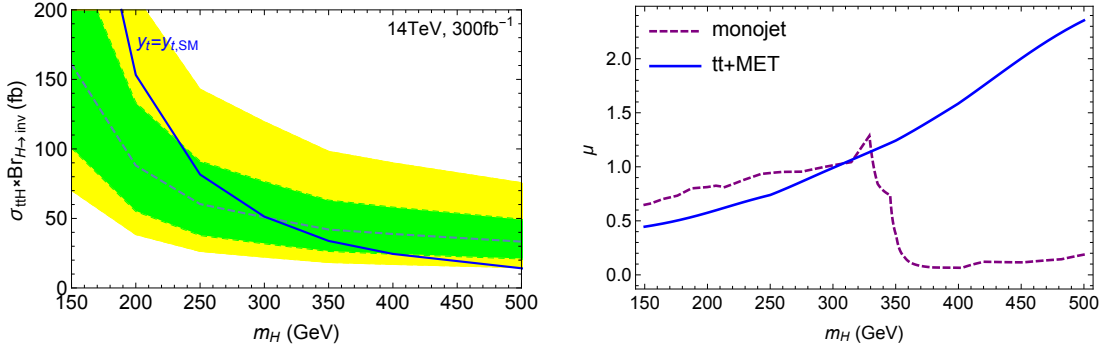


Figure 17: Left: the 14 TeV, 300 fb^{-1} expected limit on the $\sigma \times \text{Br}$ of invisibly decaying new scalars in association with top quarks. Right: comparison with the expected limit from monojet exclusion [76], both normalized to the respective SM cross sections.

5 Searching for a Charged Higgs in $t\bar{b}$

Thus far we have focused largely on the signatures of the vacuum states H and A near the alignment limit. In this section, we turn to the signatures of charged Higgs bosons H^\pm in the alignment limit, which may provide an alternative handle on 2HDM in regions of parameter space where H and A are hard to find. In particular, we analyze the LHC reach for a charged scalar H^\pm that couples to the SM top and bottom quark through a Yukawa interaction of the form

$$\mathcal{L}_{\text{eff}} = y_{tb} H^+ \bar{t} (P_L \sin \theta + P_R \cos \theta) b + \text{h.c.} \quad (5.1)$$

Near the alignment limit, $t\bar{b}$ associated production with decay to $t\bar{b}$ is the dominant channel for single production of a charged Higgs boson, as the Wh mode vanishes in the alignment limit and decays into $t\bar{b}$ swamp those into $\tau\nu$. As such, we focus on the process $pp \rightarrow H^+ t\bar{b} (H^- t\bar{b}) + X$ with $H^+ \rightarrow t\bar{b} (H^- \rightarrow t\bar{b})$, and we employ the semi-leptonic decay of the $t\bar{t}$

pair.⁵ The CMS collaboration recently published a search for the charged Higgs at 8 TeV via the same production channel, using the dileptonic decay mode of the top pair [38]; our aim is to forecast sensitivity at $\sqrt{s} = 14$ TeV and demonstrate the added sensitivity available in a semi-leptonic search. Our results are insensitive to the value of θ in Eq. (5.1), so for the results shown here we set $\theta = 0$ ⁶.

To suppress SM backgrounds, we require at least 4 b -tagged jets in the final state. The the irreducible background is

$$pp \rightarrow t\bar{t}bb, \quad (5.2)$$

while the dominant reducible backgrounds are

$$pp \rightarrow t\bar{t}bj, \quad (5.3)$$

$$pp \rightarrow t\bar{t}jj, \quad (5.4)$$

with light jets faking bottom quarks. The $t\bar{t}h$, $t\bar{t}Z$, single top production and vector boson with multijets backgrounds are comparatively negligible [61].

We generate parton level signal and backgrounds events using MadGraph5 [45] to leading order with CTEQ6L1 pdfs [59]. The events are showered with PYTHIA6.4 [55] and Delphes3 [56, 57] is used to simulate the detector.⁷ We require at least 6 jets with at least 4 b -tags, and require the leading b -jet to have $p_T > 150$ GeV. We also apply a missing transverse energy cut of $\cancel{E}_T > 30$ GeV and veto events with more than one charged lepton.

Top quarks and W bosons are reconstructed from the mass-shell constraints, with small corrections for detector effects (for details, see appendix C). After top quark reconstruction, we require that the signal events satisfy $\chi^2 < 5.0$ and $\Delta R_{b_1 b_2} > 0.9$, where χ is a variable characterizing the quality of the reconstruction (see appendix C), and b_1 (b_2) is the leading (sub-leading) b -jet which is not recognized as emerging from a top quark decay.

The charged scalar invariant mass is reconstructed from the leading b -jet and the leading reconstructed top quark. In figure 18, we show the tb invariant mass distribution of the backgrounds and the signal from a 700 GeV H^\pm with $y_{tb} = 1$ at 14 TeV LHC with 3000 fb⁻¹ integrated luminosity.

To obtain the exclusion and discovery bound, we again use the likelihood function given by Eq. (3.1), where now where x_j is the binned m_{tb} distribution predicted by the model (with or without signal) and n_j is the observed distribution. The 2σ exclusion bound is obtained

⁵Early investigation of this channel at the LHC can be found in Ref. [81].

⁶The possibility of using this channel to investigate the chirality structure of the $H^+t\bar{b}$ vertex has been studied in [82–85].

⁷Jets are reconstructed using the anti- k_T algorithm with $R = 0.5$ and are required to satisfy $p_T^j > 20$ GeV, $|\eta^j| < 4.5$. Charged leptons (electrons and muons) are required to have $p_T^\ell > 15$ GeV, $|\eta^\ell| < 2.5$, $I_{iso,\mu}(\Delta R = 0.3) < 0.1$. The b -tagging efficiency is chosen to be 70% with a 25% (2%) mistagging rate for charm (light) jets[60]. b -tagged jets satisfy $p_T^b > 40$ GeV, $|\eta^b| < 2.5$.

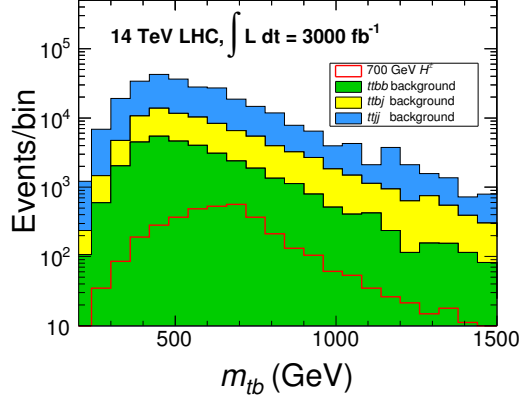


Figure 18: The tb invariant mass distribution of the backgrounds and the signal from a 700 GeV H^\pm with $y_{tb} = 1$ at 14 TeV LHC with 3000 fb^{-1} integrated luminosity.

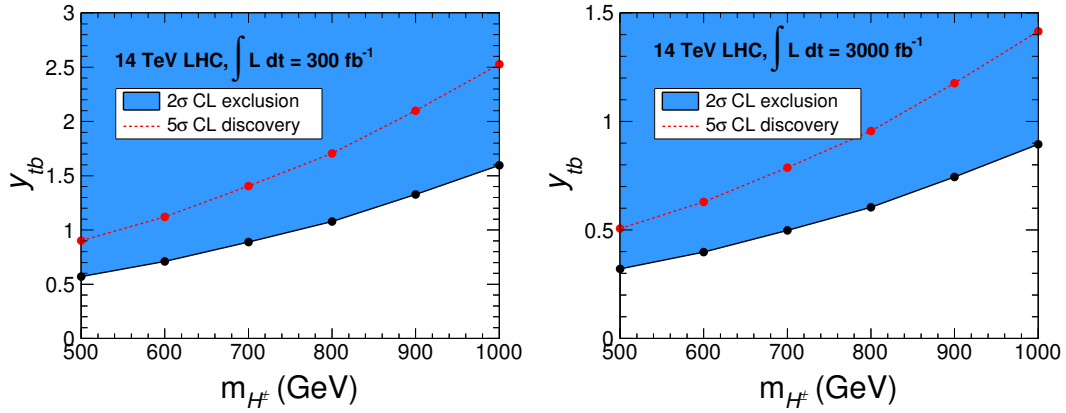


Figure 19: The 2σ exclusion and the 5σ discovery bound of the charged Higgs via searching the tb resonance in the $ttbb$ channel at 14 TeV LHC with 300 fb^{-1} (left panel) and 3000 fb^{-1} (right panel) integrated luminosity.

as in Eq. (3.2), while the 5σ discovery reach is obtained from

$$\sqrt{-2 \ln \left(\frac{L(b|\mu s + b)}{L(\mu s + b|\mu s + b)} \right)} = 5. \quad (5.5)$$

In figure 19, we show discovery and exclusion curves for the coupling constant y_{tb} as a function of m_H . We have checked that these results are insensitive to the θ angle in Eq. (5.1). In the Type 2 2HDM, Eq. (5.1) can be written as

$$\mathcal{L}_{\text{eff}} = \frac{\sqrt{2}}{v} H^+ \bar{t} (P_L m_t \cot \beta + P_R m_b \tan \beta) b + \text{h.c.} \quad (5.6)$$

As such, the constraint on y_{tb} shown in figure 19 is translated into a constraint to $\tan \beta$ in

figure 20.

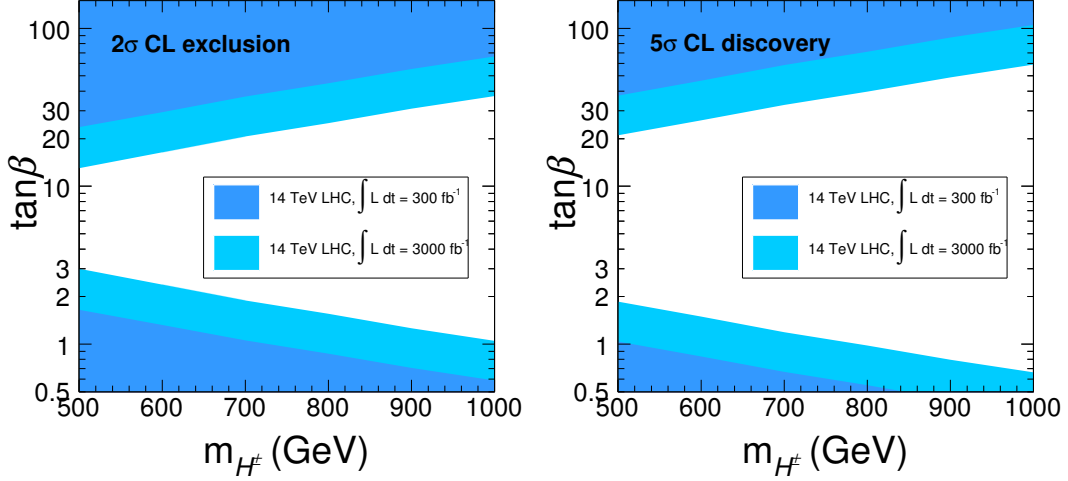


Figure 20: The 2σ exclusion (left panel) and the 5σ discovery (right panel) bound of the charged Higgs via searching the tb resonance in the $t\bar{t}b\bar{b}$ channel at 14 TeV LHC with 300 fb^{-1} and 3000 fb^{-1} integrated luminosity.

While there remains a hole in coverage at moderate values of $\tan\beta$, there is nonetheless considerable sensitivity for heavy charged Higgses in this channel at $\sqrt{s} = 14 \text{ TeV}$. Note also that the reach of the semi-leptonic search at $\sqrt{s} = 14 \text{ TeV}$ is comparable to the naive extrapolation of the $\sqrt{s} = 8 \text{ TeV}$ CMS di-leptonic search, suggesting that an optimized search for charged Higgses can effectively employ both semi-leptonic and di-leptonic final states to constrain $pp \rightarrow H^+\bar{t}b(H^-\bar{t}b) + X$ with $H^+ \rightarrow t\bar{b}(H^- \rightarrow \bar{t}b)$.

6 Conclusions

The hunt for the rest of the Higgs bosons is entering a new phase, as an ever-broadening set of direct searches at the LHC begins to constrain the parameter space of extended Higgs sectors. In this work we have attempted to identify and analyze some of the most promising open channels in existing coverage of heavy Higgs bosons consistent with properties of the observed SM-like Higgs. These channels are the production of a heavy scalar or pseudoscalar with decay to $t\bar{t}$; $b\bar{b}$ and $t\bar{t}$ and associated production of a heavy scalar or pseudoscalar with decay to invisible final states; and $t\bar{b}$ associated production of a charged Higgs with decay to $\bar{t}b$.

Heavy scalars or pseudoscalars decaying into $t\bar{t}$ constitute a significant gap in existing coverage of extended electroweak symmetry breaking scenarios. Taking into account the effects of detector resolution and $t\bar{t}$ reconstruction, we have found that searches for resonant production of heavy Higgses with decay into $t\bar{t}$ are likely to be systematics-limited at the LHC. We have correspondingly proposed several ancillary channels involving associated production

that may provide complementary sensitivity. The most promising is $t\bar{t}H/A$ production with $H/A \rightarrow t\bar{t}$.

Searches involving missing energy provide an effective probe of intriguing scenarios where a heavy Higgs decays invisibly. We demonstrated that $b\bar{b}H/A$ and $t\bar{t}H/A$ are valuable production channels in which to search for $H/A \rightarrow \text{inv}$. Furthermore, their reach is expected to be competitive with – or better than – monojet searches in some models and mass ranges.

Finally, heavy charged Higgses in the alignment limit decay dominantly to tb if this channel is open, and the natural strong production channel for charged Higgses with $m_{H^\pm} \geq m_t + m_b$ is in association with tb . We studied the reach in the semileptonic channel, where the system can be completely reconstructed, and find considerable sensitivity to heavy charged Higgses that can complement existing searches in the dileptonic channel.

In conjunction with precision Higgs coupling measurements and existing direct searches for heavy Higgs bosons, these searches can maximize the LHC discovery potential for the most well-motivated extensions of the Higgs sector.

Acknowledgments

We thank Duane Dicus, John Paul Chou, Yuri Gershtein, and Sunil Somalwar for useful conversations. H. Zhang is supported by the U.S. DOE under contract No. DE-SC0011702. S. Thomas is supported by the U.S. DOE under grant DE-SC0010008.

A Higgs Couplings Fit

We consider only a single SM-like Higgs boson of mass $m_h = 125$ GeV whose couplings to SM fermions and gauge bosons are modified relative to an SM Higgs boson of the same mass by coupling modifiers $\kappa_i \equiv g_i/g_{i,SM}$, where $i = t, b, \tau, W, Z, g, \gamma$. We treat the loop-induced couplings to gluons and photons independently from variations in the fermion couplings to allow for new degrees of freedom running in loops. For simplicity we assume custodial symmetry so that $\kappa_Z = \kappa_W$. We do not consider a potential invisible width or couplings with non-SM tensor structure.

We construct likelihoods for a Higgs coupling fit using data from Higgs analyses reported by the ATLAS and CMS collaborations. Single-channel likelihoods are constructed for each Higgs analysis using a two-sided Gaussian where the central value corresponds to the best-fit signal strength modifier $\hat{\mu}$ reported in the analysis and the variance on each side corresponds to the 1σ error on the signal strength modifier, i.e.

$$\mathcal{L}_i^\pm(\mu) \propto \exp\left[\frac{-(\mu - \hat{\mu}_i)^2}{2(\sigma_i^\pm)^2}\right]. \quad (\text{A.1})$$

This two-sided likelihood accommodates the often sizable non-gaussianities found in low-statistics channels.

The theory prediction for the signal strength modifier μ is constructed by summing over the production and decay modes considered in the analysis (each of which is a function of the coupling modifiers κ_i), weighted by the relative contribution ϵ of each production mode to the analysis. These relative contributions are extracted from experimental publications or inferred from the literature where appropriate. We neglect uncertainties on the values of ϵ . We consider experimental analyses for which a single decay mode dominates the analysis, so that the signal strength modifier for a single experimental channel is given by

$$\mu = \left(\sum_a \epsilon_a \frac{\sigma_a}{\sigma_{a,SM}} \right) \frac{BR}{BR_{SM}}, \quad (\text{A.2})$$

where the index a runs over the gluon fusion, vector boson fusion & associated vector production, and associated $t\bar{t}$ production modes. The set of ATLAS and CMS Higgs analyses used to construct our coupling fit (with corresponding best-fit signal strength modifiers, 1σ errors, and relative efficiencies) are enumerated in tables 5 and 6.

Channel	\sqrt{s}	$\hat{\mu}_a$	$\epsilon_a(\text{GGH, VBF/VH, TTH})$
$Vh \rightarrow b\bar{b}$ (0 ℓ) [86]	7/8 TeV	$-0.35^{+0.55}_{-0.52}$	(0.0, 1.0, 0.0)
$Vh \rightarrow b\bar{b}$ (1 ℓ) [86]	7/8 TeV	$1.17^{+0.66}_{-0.60}$	(0.0, 1.0, 0.0)
$Vh \rightarrow b\bar{b}$ (2 ℓ) [86]	7/8 TeV	$0.94^{+0.88}_{-0.79}$	(0.0, 1.0, 0.0)
$tth \rightarrow b\bar{b}$ [87]	7/8 TeV	$1.7^{+1.4}_{-1.4}$	(0.0, 0.0, 1.0)
$h \rightarrow \tau\tau$ (jj) [88]	7/8 TeV	$3.6^{+2.0}_{-1.6}$	(0.60, 0.4, 0.0)
$h \rightarrow \tau\tau$ (ℓj) [88]	7/8 TeV	$0.9^{+1.0}_{-0.9}$	(0.65, 0.35, 0.0)
$h \rightarrow \tau\tau$ ($\ell\ell$) [88]	7/8 TeV	$3.0^{+1.9}_{-1.7}$	(0.65, 0.35, 0.0)
$hjj \rightarrow \tau\tau$ (jj) [88]	7/8 TeV	$1.4^{+0.9}_{-0.7}$	(0.15, 0.85, 0.0)
$hjj \rightarrow \tau\tau$ (ℓj) [88]	7/8 TeV	$1.0^{+0.6}_{-0.5}$	(0.12, 0.88, 0.0)
$hjj \rightarrow \tau\tau$ ($\ell\ell$) [88]	7/8 TeV	$1.8^{+1.1}_{-0.9}$	(0.10, 0.90, 0.0)
$h \rightarrow WW$ (0 j) [89]	7/8 TeV	$1.14^{+0.34}_{-0.30}$	(0.98, 0.02, 0.0)
$h \rightarrow WW$ (1 j) [89]	7/8 TeV	$0.96^{+0.45}_{-0.40}$	(0.87, 0.13, 0.0)
$h \rightarrow WW$ (2 j ggH) [89]	7/8 TeV	$1.20^{+0.91}_{-0.84}$	(0.75, 0.25, 0.0)
$h \rightarrow WW$ (2 j VBF) [89]	7/8 TeV	$1.20^{+0.45}_{-0.38}$	(0.13, 0.87, 0.0)
$h \rightarrow ZZ$ (ggH) [90]	7/8 TeV	$1.66^{+0.5}_{-0.4}$	(1.0, 0.0, 0.0)
$h \rightarrow ZZ$ (VBF+VH)[90]	7/8 TeV	$0.26^{+1.6}_{-0.9}$	(0.0, 1.0, 0.0)
$h \rightarrow \gamma\gamma$ (ggH) [91]	7/8 TeV	$1.32^{+0.38}_{-0.38}$	(1.0, 0.0, 0.0)
$h \rightarrow \gamma\gamma$ (VBF) [91]	7/8 TeV	$0.8^{+0.7}_{-0.7}$	(0.0, 1.0, 0.0)
$h \rightarrow \gamma\gamma$ (WH) [91]	7/8 TeV	$1.0^{+1.6}_{-1.6}$	(0.0, 1.0, 0.0)
$h \rightarrow \gamma\gamma$ (ZH) [91]	7/8 TeV	$0.1^{+3.7}_{-0.1}$	(0.0, 1.0, 0.0)
$h \rightarrow \gamma\gamma$ (ttH) [91]	7/8 TeV	$1.6^{+2.7}_{-1.8}$	(0.0, 0.0, 1.0)

Table 5: ATLAS Higgs analyses used in constructing coupling fits. The best-fit signal strength modifier is denoted by $\hat{\mu}$ with corresponding $\pm 1\sigma$ errors. The relative contributions ϵ are reported for production initiated by gluons via gluon fusion (GGH), weak gauge bosons via vector boson fusion or vector associated production (VBF/VH), and top quarks via $t\bar{t}$ associated production (TTH).

Channel	\sqrt{s}	$\hat{\mu}_a$	$\epsilon_a(\text{GGH, VBF/VH, TTH})$
$h \rightarrow bb$ [92]	7/8 TeV	$1.0^{+0.53}_{-0.50}$	(0.0, 1.0, 0.0)
$tth \rightarrow bb$ [93]	7/8 TeV	$0.67^{+1.35}_{-1.33}$	(0.0, 0.0, 1.0)
$h \rightarrow \tau\tau$ (0,1j) [92]	7/8 TeV	$0.84^{+0.42}_{-0.38}$	(0.87, 0.13, 0.0)
$hjj \rightarrow \tau\tau$ (2j) [92]	7/8 TeV	$0.95^{+0.43}_{-0.38}$	(.17, .83, 0.0)
$Vh \rightarrow \tau\tau$ [92]	7/8 TeV	$0.87^{+1.00}_{-0.88}$	(0.0, 1.0, 0.0)
$h \rightarrow WW$ (0,1j) [92]	7/8 TeV	$0.77^{+0.23}_{-0.21}$	(0.83, 0.17, 0.0)
$h \rightarrow WW$ (2j) [92]	7/8 TeV	$0.62^{+0.59}_{-0.48}$	(0.17, 0.83, 0.0)
$Vh \rightarrow WW$ [92]	7/8 TeV	$0.80^{+1.09}_{-0.93}$	(0.0, 1.00, 0.0)
$h \rightarrow ZZ$ [92]	7/8 TeV	$0.88^{+0.34}_{-0.27}$	(0.9, 0.1, 0.0)
$h \rightarrow ZZ$ (2j) [92]	7/8 TeV	$1.55^{+0.95}_{-0.66}$	(0.58, 0.42, 0.0)
$h \rightarrow \gamma\gamma$ (ggH) [94]	7/8 TeV	$1.12^{+0.37}_{-0.32}$	(1.0, 0.0, 0.0)
$h \rightarrow \gamma\gamma$ (VBF) [94]	7/8 TeV	$1.58^{+0.77}_{-0.68}$	(0.0, 1.0, 0.0)
$h \rightarrow \gamma\gamma$ (VH) [94]	7/8 TeV	$-0.16^{+1.16}_{-0.79}$	(0.0, 1.0, 0.0)
$h \rightarrow \gamma\gamma$ (ttH) [94]	7/8 TeV	$2.69^{+2.51}_{-1.81}$	(0.0, 0.0, 1.0)

Table 6: CMS Higgs analyses used in constructing coupling fits. The best-fit signal strength modifier is denoted by $\hat{\mu}$ with corresponding $\pm 1\sigma$ errors. The relative contributions ϵ are reported for production initiated by gluons via gluon fusion (GGH), weak gauge bosons via vector boson fusion or vector associated production (VBF/VH), and top quarks via $t\bar{t}$ associated production (TTH).

We construct a combined likelihood from the product of all single-channel likelihoods,

$$\mathcal{L}(\mu) = \prod_i \mathcal{L}_i(\mu). \quad (\text{A.3})$$

This approach does not take into account correlations among systematic uncertainties in different Higgs searches, as such information is not publicly available. However, this is a reasonable approximation since uncertainties in Higgs measurements are not yet dominated by systematics. We are often interested in treating some inputs as nuisance parameters θ , in which case the combined likelihood may be expressed as a function of both μ and θ .

We construct coupling fits using the profile likelihood approach [62]. In this approach, the best-fit signal strength modifier $\hat{\mu}$ and corresponding uncertainty $\Delta\hat{\mu}$ of the combined likelihood are calculated using the likelihood ratio $\lambda(\mu) = \mathcal{L}(\mu, \hat{\theta}) / \mathcal{L}(\hat{\mu}, \hat{\theta})$. This is the ratio of a likelihood function with nuisance parameters $\hat{\theta}$ optimized for a given value of μ to a likelihood function where $\hat{\mu}$ and $\hat{\theta}$ are optimized simultaneously. Optimizing nuisance parameters $\hat{\theta}$ for a given value of μ amounts to profiling these nuisance parameters. Given this likelihood ratio, the uncertainty $\Delta\hat{\mu}$ is computed using the test statistic $-2 \ln \lambda(\mu)$, which converges to a χ^2 distribution in one degree of freedom as the data sample size is taken to be large.

B The $gg \rightarrow H/A \rightarrow t\bar{t}$ Differential Cross Section

The kinematics of spin averaged two to two on-shell scattering processes $12 \rightarrow 34$ are completely specified by the masses of the particles, energy-momentum conservation, and the Mandelstam variables $s = (p_1 + p_2)^2$ and $t = (p_1 - p_3)^2$. In order to characterize the invariant phase space distribution for these processes it is useful to define a shifted dimensionless version of the Mandelstam variable t that has a flat metric with respect to the squared amplitude. For $m_1 = m_2 = 0$ and $m_3 = m_4 = m$ this variable is

$$\varpi = 1 + \frac{2}{s}(t - m^2) = \beta \cos \theta = \tanh\left(\frac{y_3 - y_4}{2}\right) \quad (\text{B.1})$$

where $\beta = \sqrt{1 - 4m^2/s}$ is the velocity of either final state particle in the center of mass frame, $\cos \theta$ is the cosine of the center of mass scattering angle, and $y = \tanh^{-1}(p_z/E)$ are the individual rapidities of the final state particles in any longitudinal frame. The scattering variable lies in the range $-\beta \leq \varpi \leq \beta$. At fixed s the differential cross section with respect to ϖ and t and $\cos \theta$ are related by

$$\frac{d\sigma}{d\varpi} = \frac{s}{2} \frac{d\sigma}{dt} = \frac{1}{\beta} \frac{d\sigma}{d\cos \theta} \quad (\text{B.2})$$

Experimentally the variable ϖ is more robust than $\cos \theta$ near threshold since $\beta \rightarrow 0$ and $\cos \theta$ becomes ill-defined at threshold, but $\varpi \rightarrow 1$ in this limit. In addition, $s d\sigma/d\varpi$ is proportional to the dimensionless scattering amplitude squared everywhere in phase space. So the dimensionless coordinates ϖ and $x^2 = s/(4m^2)$ provide a flat metric for the probability density in phase space, with the physical phase space region given by $x^2 \geq 1$ and $-\sqrt{1 - 1/x^2} \leq \varpi \leq \sqrt{1 - 1/x^2}$. Central scattering corresponds to $\varpi = 0$. The phase space volume vanishes at threshold, $x^2 = 1$, $\varpi = 0$. These coordinates for two to two scattering are the analogs of Dalitz coordinates for three-body decay.

For heavy scalar and pseudo-scalar Higgs bosons with masses greater than twice the top quark mass, $m_H, m_A > 2m_t$, the scattering of two gluons to a top and anti-top quark, $gg \rightarrow t\bar{t}$, receives contributions both from QCD interactions, as well as from s -channel gluon fusion production and decay of H and A . The differential cross section including all these processes is given by [39]

$$s \frac{d\sigma}{d\varpi}(gg \rightarrow t\bar{t}) = \frac{7\pi\alpha_s^2}{96} \left[f(s/4m_t^2, \varpi)_{\text{QCD}} + f(s/4m_t^2, s/4m_b^2, m_H^2/m_t^2, \varpi)_{\text{H-QCD}} \right. \\ \left. + f(s/4m_t^2, s/4m_b^2, m_A^2/m_t^2, \varpi)_{\text{A-QCD}} + f(s/4m_t^2, s/4m_b^2, m_H^2/m_t^2, \varpi)_{\text{H}} \right. \\ \left. + f(s/4m_t^2, s/4m_b^2, m_A^2/m_t^2, \varpi)_{\text{A}} \right] \quad (\text{B.3})$$

where

$$\begin{aligned}
f(x_t^2, \varpi)_{\text{QCD}} &= \frac{7 + 9\varpi^2}{7(1 - \varpi^2)} \left(\frac{1}{1 + \varpi^2} + \frac{2}{x_t^2} - \frac{2}{x_t^4(1 - \varpi^2)} \right) \\
f(x_t^2, x_b^2, r^2, \varpi)_{\text{H-QCD}} &= -\frac{24}{7(1 - \varpi^2)} \left(1 - \frac{1}{x_t^2} \right) \text{Re} \left[\frac{[4x_t^2 - r^2 - 4ix_t^2\gamma_H(x_t)]\tilde{N}(x_t^2, x_b^2)}{(4x_t^2 - r^2)^2 + 16x_t^4\gamma_H^2(x_t)} \right] \\
f(x_t^2, x_b^2, r^2, \varpi)_{\text{A-QCD}} &= -\frac{6}{7(1 - \varpi^2)^2} \text{Re} \left[\frac{[4x_t^2 - r^2 - 4ix_t^2\gamma_A(x_t)]\tilde{P}(x_t^2, x_b^2)}{(4x_t^2 - r^2)^2 + 16x_t^4\gamma_A^2(x_t)} \right] \\
f(x_t^2, x_b^2, r^2, \varpi)_{\text{H}} &= \frac{72x_t^2}{7} \left(1 - \frac{1}{x_t^2} \right) \frac{\left| [4x_t^2 - r^2 - 4ix_t^2\gamma_H(x_t)]\tilde{N}(x_t^2, x_b^2) \right|^2}{\left[(4x_t^2 - r^2)^2 + 16x_t^4\gamma_H^2(x_t) \right]^2} \\
f(x_t^2, x_b^2, r^2, \varpi)_{\text{A}} &= \frac{72x_t^2}{112} \frac{\left| [4x_t^2 - r^2 - 4ix_t^2\gamma_H(x_t)]\tilde{P}(x_t^2, x_b^2) \right|^2}{\left[(4x_t^2 - r^2)^2 + 16x_t^4\gamma_A^2(x_t) \right]^2} \tag{B.4}
\end{aligned}$$

The first term for the QCD scattering amplitude squared function is unity for central scattering both at and well above threshold where $f(1, 0)_{\text{QCD}} = f(\infty, 0)_{\text{QCD}} = 1$. The second and third terms arise from interference between the heavy scalar and pseudo-scalar Higgs s -channel amplitudes and the spin and color singlet component of the QCD amplitude. Near threshold the scalar Higgs amplitude interferes with the P -wave component of the QCD amplitude, while the pseudo-scalar amplitude interferes with the S -wave component. These terms include one-loop functions for the gluon fusion production amplitudes generated by top and bottom quark loops

$$\begin{aligned}
\tilde{N}(x_t^2, x_b^2) &= \frac{\sqrt{2}G_F}{4\pi^2} m_t\kappa_t^H \sum_{f=t,b} m_f\kappa_f^H \left[1 - \frac{1}{4} \left(1 - \frac{1}{x_f^2} \right) \left(\ln \frac{1 + \sqrt{1 - 1/x_f^2}}{1 - \sqrt{1 - 1/x_f^2}} - i\pi \right)^2 \right] \\
\tilde{P}(x_t^2, x_b^2) &= -\frac{\sqrt{2}G_F}{4\pi^2} m_t\kappa_t^A \sum_{f=t,b} m_f\kappa_f^A \left(\ln \frac{1 + \sqrt{1 - 1/x_f^2}}{1 - \sqrt{1 - 1/x_f^2}} - i\pi \right)^2 \tag{B.5}
\end{aligned}$$

The $i\pi$ terms come from absorptive branch cuts in the one-loop amplitudes. For the top quark loop contributions to the full amplitude, these absorptive pieces represent QCD production of an on-shell top and anti-top quark with final state re-scattering through intermediate s -channel heavy Higgs bosons. For $m_H = m_A \gg m_t$ the absorptive contributions to the interference of the heavy scalar and pseudo-scalar Higgs bosons with QCD are equal in both magnitude and sign for all center of mass scattering energies. Away from the heavy Higgs resonances, interference of the QCD and non-absorptive parts of the heavy Higgs amplitudes are suppressed compared with the QCD amplitude squared by $\mathcal{O}(\lambda_t\lambda_f/4\pi^2)$ where $f = t, b$. The functional dependence of the interference terms on the angular scattering variable ϖ

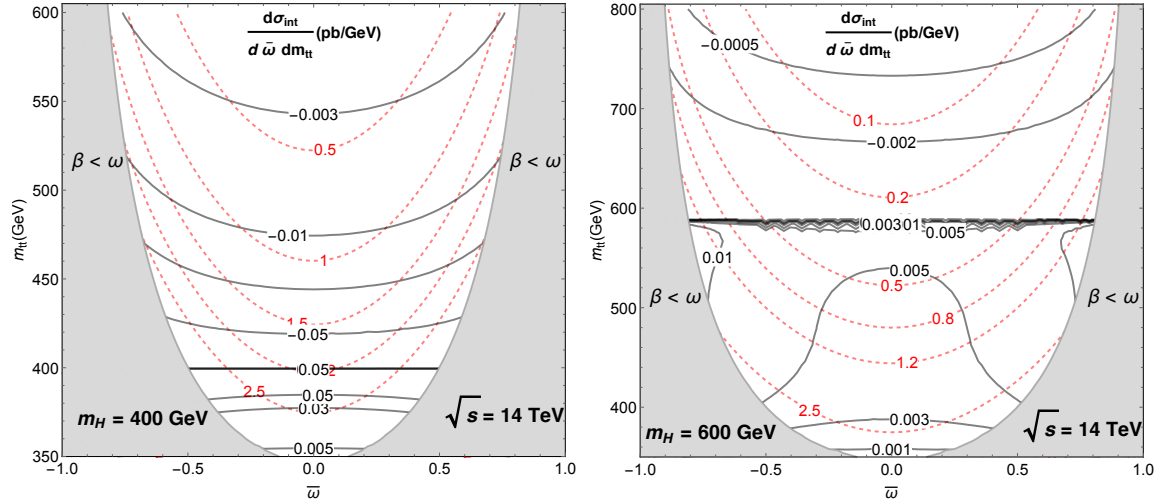


Figure 21: Isocontours for the differential cross sections $d^2\sigma/d\varpi dm_{t\bar{t}}$ in QCD (red dotted lines) and for the interference terms in QCD+H (black solid lines) at 14 TeV with $\kappa_t^H = 1$. The left (right) panel shows the results for $m_H = 400$ (600) GeV.

is universal and independent of the center of mass scattering energy. The real part of the interference terms changes sign across the resonances, leading to a distinctive excess below, and deficit above, the resonances [39]. The fourth and fifth terms arise from the square of the amplitudes for s -channel production and decay of the heavy Higgs bosons. Away from the heavy Higgs resonances, the non-absorptive parts of the heavy Higgs amplitudes squared are suppressed compared with the QCD amplitude squared by $\mathcal{O}(\lambda_t^2 \lambda_f^2 / 16\pi^4)$ where $f = t, b$. The running dimensionless widths of the heavy Higgs bosons are

$$\gamma_X(x) = \frac{\Gamma_X(s)}{\sqrt{s}} \quad (\text{B.6})$$

where $\Gamma_X = \Gamma(X \rightarrow \text{All})$ are the running total widths for $X = H, A$. These terms in the s -channel heavy Higgs propagators represent absorptive final state re-scattering of the heavy Higgs bosons through all intermediate on-shell states that contribute to the Higgs boson decay widths.

The scalar and pseudo-scalar Higgs amplitudes do not interfere in the spin averaged top and anti-top quark production differential cross section. Interference could arise first in a spin averaged production differential cross section with at least two gluons radiated from the final state. It also arises in the spin averaged differential cross section of the full phase of the top and anti-top quark decay products.

In Fig. 21 we plot contours of the differential $gg \rightarrow t\bar{t}$ cross section $d^2\sigma/d\varpi dm_{t\bar{t}}$ in QCD and of the interference contribution in QCD with a heavy scalar Higgs boson. We see that although the angular scattering variable offers some distinctive discrimination, there is no

region where magnitude of this discrimination is able to effectively overcome the prodigious QCD background.

C Top Quark Reconstruction

In the $H/A \rightarrow t\bar{t}$, $b\bar{b}H/A \rightarrow b\bar{b}t\bar{t}$, and charged Higgs analyses, we reconstruct the W bosons and top quarks with the following algorithm.

The hadronically-decaying W boson is reconstructed using the non- b -tagged jets in the events. We choose the pair of the jets j_1j_2 which minimizes $|m_{j_1j_2} - m_{Wh}|$, where $m_{j_1j_2}$ is the invariant mass of the dijet system and $m_{Wh} = 77.5$ GeV.⁸ The reconstructed hadronic decaying W 4-momentum is rescaled by a small correction factor of m_W/m_{Wh} , where $m_W = 80.4$ GeV.

To reconstruct the leptonically-decaying top quark, we solve for the 4-momentum of the neutrino in the final state using neutrino and W mass shell conditions. The solution for the z -component of the neutrino momentum is

$$p_{\nu L}^{\pm} = \frac{A(m_W) p_{\ell L} \pm E_{\ell} \sqrt{A(m_W)^2 - 4p_{\ell T}^2 \vec{E}_T^2}}{2p_{\ell T}^2} \quad (\text{C.1})$$

where $A(m_W) \equiv m_W^2 + 2\vec{p}_{\ell T} \cdot \vec{E}_T$. When there are two real solutions, the mass-shell condition of the top quark may be used to select the “true” solution. Due to detector smearing effects and the finite width, there may be no real solution for $p_{\nu L}$. For such events with negative discriminant, we enforce

$$A(m_W) = \pm 2p_{\ell T} \vec{E}_T \quad (\text{C.2})$$

and look for a modified \vec{E}_T' which minimizes $(\vec{E}_T' - \vec{E}_T)^2$. It is clear that when $\vec{p}_{\ell T}$ is parallel to \vec{E}_T , the discriminant must be positive. So we can expand

$$\vec{E}_T' = x\vec{p}_{\ell T} + (1+y)\vec{E}_T. \quad (\text{C.3})$$

Then we have a constrained minimum value problem, which can be solved with Lagrange multipliers. We obtain a cubic surface and with a unique real solution

$$y = -\frac{\left[d^2 - (5m_W^2 + 4c)d + (m_W^2 - 4c)^2\right]}{\left[d^2 + (m_W^2 - 4c)d + (m_W^2 - 4c)^2\right]}, \quad (\text{C.4})$$

$$x = -\frac{\left[d^2 + (m_W^2 + 8c)d + (m_W^2 - 4c)^2\right]y}{12ad}, \quad (\text{C.5})$$

⁸ m_{Wh} is the center of the $m_{j_1j_2}$ distribution obtained from the simulation of a pure sample of hadronic- W events.

where

$$a = \vec{p}_{\ell T}^2, \tag{C.6}$$

$$b = \vec{E}_T^2, \tag{C.7}$$

$$c = \vec{p}_{\ell T} \cdot \vec{E}_T, \tag{C.8}$$

$$d = \{216abm_W^2 + (m_W^2 + 8c)(m_W^4 - 20m_W^2c - 8c^2) \\ + 12\sqrt{3}m_W [108abm_W^2 + (m_W^2 + 2c)^2(m_W^2 - 16c)]^{1/2} \\ \times (ab - c^2)^{1/2}\}^{1/3}. \tag{C.9}$$

We show the correction to the missing transverse momentum in figure 22. It is evident that

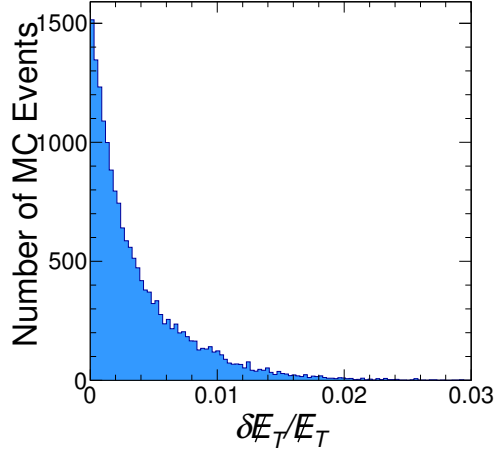


Figure 22: The correction to the missing transverse momentum used to obtain a real solution to the mass shell equation for the leptonically-decaying W boson.

for most of the events with negative discriminant we only need to shift the missing transverse momentum by a factor of order 1%.

To reconstruct the top quarks in the final state, we try all of the combinations $(W_h b_h)(W_\ell b_\ell)$, where W_h and W_ℓ are the reconstructed hadronic and leptonic W bosons and b_h and b_ℓ are b -tagged jets in the event. When there are two different real solutions of the neutrino longitudinal momentum, both of them are used. We select the combination which minimizes

$$\chi^2 = \frac{(m_{W_h b_h} - m_t)^2}{\sigma_h^2} + \frac{(m_{W_\ell b_\ell} - m_t)^2}{\sigma_\ell^2}, \tag{C.10}$$

where $m_t = 173.2$ GeV is the pole mass of the top quark, $\sigma_h = 50$ GeV and $\sigma_\ell = 25$ GeV. To check the reconstruction efficiency, we compare the reconstructed top quark 4-momenta with the real parton-level momenta in the corresponding event. We calculate the ratio of

the modulus of the reconstructed top quark 3-momentum in the corresponding parton-level top quark rest frame to the energy of the parton-level top quark in the laboratory frame, $\delta p_{t_{h(l)}}/E_{t_{h(l)}}$. The result is shown in figure 23 (note the logarithmic z-axis). It is clear that most of the reconstructed top quarks fall in the $\delta p/E < 0.15$ region, meaning the top quarks in the events are well-reconstructed.

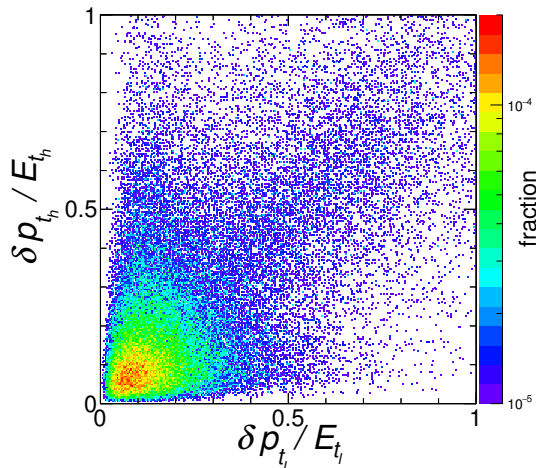


Figure 23: The 2-dimensional distribution of the reconstruction efficiency of the hadronic and leptonic decaying top quarks in the events.

References

- [1] **ATLAS** Collaboration, G. Aad et al., *Search for a CP-odd Higgs boson decaying to Zh in pp collisions at $\sqrt{s} = 8$ TeV with the ATLAS detector*, *Phys.Lett.* **B744** (2015) 163–183, [[arXiv:1502.04478](#)].
- [2] **ATLAS** Collaboration, G. Aad et al., *Search for a Charged Higgs Boson Produced in the Vector-boson Fusion Mode with Decay $H^\pm \rightarrow W^\pm Z$ using pp Collisions at $\sqrt{s} = 8$ TeV with the ATLAS Experiment*, [[arXiv:1503.04233](#)].
- [3] **ATLAS** Collaboration, G. Aad et al., *Search for the Standard Model Higgs boson in the decay channel $H \rightarrow ZZ(*) \rightarrow 4\ell$ with 4.8 fb⁻¹ of pp collision data at $\sqrt{s} = 7$ TeV with ATLAS*, *Phys.Lett.* **B710** (2012) 383–402, [[arXiv:1202.1415](#)].
- [4] **CMS** Collaboration, S. Chatrchyan et al., *Search for a standard-model-like Higgs boson with a mass in the range 145 to 1000 GeV at the LHC*, *Eur.Phys.J.* **C73** (2013) 2469, [[arXiv:1304.0213](#)].
- [5] **CMS** Collaboration, “Search for a pseudoscalar boson A decaying into a Z and an h boson in the llbb final state.” CMS-PAS-HIG-14-011, 2014.
- [6] **CMS** Collaboration, V. Khachatryan et al., *Search for a Higgs boson in the mass range from 145 to 1000 GeV decaying to a pair of W or Z bosons*, [[arXiv:1504.00936](#)].

- [7] **CMS** Collaboration, V. Khachatryan et al., *Searches for heavy Higgs bosons in two-Higgs-doublet models and for $t \rightarrow ch$ decay using multilepton and diphoton final states in pp collisions at 8 TeV*, *Phys.Rev.* **D90** (2014) 112013, [[arXiv:1410.2751](#)].
- [8] **ATLAS** Collaboration, G. Aad et al., *Search for neutral Higgs bosons of the minimal supersymmetric standard model in pp collisions at $\sqrt{s} = 8$ TeV with the ATLAS detector*, *JHEP* **1411** (2014) 056, [[arXiv:1409.6064](#)].
- [9] **CMS** Collaboration, V. Khachatryan et al., *Search for neutral MSSM Higgs bosons decaying to a pair of tau leptons in pp collisions*, *JHEP* **1410** (2014) 160, [[arXiv:1408.3316](#)].
- [10] S. Dube, J. Glatzer, S. Somalwar, A. Sood, and S. Thomas, *Addressing the Multi-Channel Inverse Problem at High Energy Colliders: A Model Independent Approach to the Search for New Physics with Trileptons*, *J.Phys.* **G39** (2012) 085004, [[arXiv:0808.1605](#)].
- [11] J. Alwall, P. Schuster, and N. Toro, *Simplified Models for a First Characterization of New Physics at the LHC*, *Phys.Rev.* **D79** (2009) 075020, [[arXiv:0810.3921](#)].
- [12] **LHC New Physics Working Group** Collaboration, D. Alves et al., *Simplified Models for LHC New Physics Searches*, *J.Phys.* **G39** (2012) 105005, [[arXiv:1105.2838](#)].
- [13] N. Craig and S. Thomas, *Exclusive Signals of an Extended Higgs Sector*, *JHEP* **1211** (2012) 083, [[arXiv:1207.4835](#)].
- [14] N. Craig, J. Galloway, and S. Thomas, *Searching for Signs of the Second Higgs Doublet*, [[arXiv:1305.2424](#)].
- [15] M. Carena, I. Low, N. R. Shah, and C. E. Wagner, *Impersonating the Standard Model Higgs Boson: Alignment without Decoupling*, *JHEP* **1404** (2014) 015, [[arXiv:1310.2248](#)].
- [16] H. E. Haber, *The Higgs data and the Decoupling Limit*, [[arXiv:1401.0152](#)].
- [17] J. F. Gunion and H. E. Haber, *The CP conserving two Higgs doublet model: The Approach to the decoupling limit*, *Phys.Rev.* **D67** (2003) 075019, [[hep-ph/0207010](#)].
- [18] P. B. Dev and A. Pilaftsis, *Maximally Symmetric Two Higgs Doublet Model with Natural Standard Model Alignment*, *JHEP* **1412** (2014) 024, [[arXiv:1408.3405](#)].
- [19] D. Das and I. Saha, *Search for a 'stable alignment limit' in two Higgs-doublet models*, [[arXiv:1503.02135](#)].
- [20] P. S. B. Dev and A. Pilaftsis, *Natural Standard Model Alignment in the Two Higgs Doublet Model*, [[arXiv:1503.09140](#)].
- [21] S. L. Glashow and S. Weinberg, *Natural Conservation Laws for Neutral Currents*, *Phys.Rev.* **D15** (1977) 1958.
- [22] A. Celis, V. Ilisie, and A. Pich, *LHC constraints on two-Higgs doublet models*, *JHEP* **1307** (2013) 053, [[arXiv:1302.4022](#)].
- [23] C.-W. Chiang and K. Yagyu, *Implications of Higgs boson search data on the two-Higgs doublet models with a softly broken Z_2 symmetry*, *JHEP* **1307** (2013) 160, [[arXiv:1303.0168](#)].
- [24] B. Grinstein and P. Uttayarat, *Carving Out Parameter Space in Type-II Two Higgs Doublets Model*, *JHEP* **1306** (2013) 094, [[arXiv:1304.0028](#)].

- [25] C.-Y. Chen, S. Dawson, and M. Sher, *Heavy Higgs Searches and Constraints on Two Higgs Doublet Models*, *Phys.Rev.* **D88** (2013), no. 3 015018, [[arXiv:1305.1624](#)].
- [26] G. Belanger, B. Dumont, U. Ellwanger, J. Gunion, and S. Kraml, *Global fit to Higgs signal strengths and couplings and implications for extended Higgs sectors*, *Phys.Rev.* **D88** (2013) 075008, [[arXiv:1306.2941](#)].
- [27] V. Barger, L. L. Everett, H. E. Logan, and G. Shaughnessy, *Scrutinizing the 125 GeV Higgs boson in two Higgs doublet models at the LHC, ILC, and Muon Collider*, *Phys.Rev.* **D88** (2013), no. 11 115003, [[arXiv:1308.0052](#)].
- [28] E. Brownson, N. Craig, U. Heintz, G. Kukartsev, M. Narain, et al., *Heavy Higgs Scalars at Future Hadron Colliders (A Snowmass Whitepaper)*, [arXiv:1308.6334](#).
- [29] C.-Y. Chen, *Projections for Two Higgs Doublet Models at the LHC and ILC: A Snowmass White Paper*, [arXiv:1308.3487](#).
- [30] S. Chang, S. K. Kang, J.-P. Lee, K. Y. Lee, S. C. Park, et al., *Two Higgs doublet models for the LHC Higgs boson data at $\sqrt{s} = 7$ and 8 TeV*, *JHEP* **1409** (2014) 101, [[arXiv:1310.3374](#)].
- [31] K. Cheung, J. S. Lee, and P.-Y. Tseng, *Higgcision in the Two-Higgs Doublet Models*, *JHEP* **1401** (2014) 085, [[arXiv:1310.3937](#)].
- [32] A. Celis, V. Ilisie, and A. Pich, *Towards a general analysis of LHC data within two-Higgs-doublet models*, *JHEP* **1312** (2013) 095, [[arXiv:1310.7941](#)].
- [33] C. Englert, A. Freitas, M. Mhlleitner, T. Plehn, M. Rauch, et al., *Precision Measurements of Higgs Couplings: Implications for New Physics Scales*, *J.Phys.* **G41** (2014) 113001, [[arXiv:1403.7191](#)].
- [34] B. Dumont, J. F. Gunion, Y. Jiang, and S. Kraml, *Constraints on and future prospects for Two-Higgs-Doublet Models in light of the LHC Higgs signal*, *Phys.Rev.* **D90** (2014), no. 3 035021, [[arXiv:1405.3584](#)].
- [35] S. Kanemura, K. Tsumura, K. Yagyu, and H. Yokoya, *Fingerprinting nonminimal Higgs sectors*, *Phys.Rev.* **D90** (2014) 075001, [[arXiv:1406.3294](#)].
- [36] M. Carena, H. E. Haber, I. Low, N. R. Shah, and C. E. M. Wagner, *Complementarity between nonstandard Higgs boson searches and precision Higgs boson measurements in the MSSM*, *Phys.Rev.* **D91** (2015), no. 3 035003, [[arXiv:1410.4969](#)].
- [37] A. Djouadi, L. Maiani, A. Polosa, J. Quevillon, and V. Riquer, *Fully covering the MSSM Higgs sector at the LHC*, [arXiv:1502.05653](#).
- [38] **CMS** Collaboration, CMS, “Search for a heavy charged Higgs boson in proton-proton collisions at $\sqrt{s}=8$ TeV with the CMS detector.” CMS-PAS-HIG-13-026, 2014.
- [39] D. Dicus, A. Stange, and S. Willenbrock, *Higgs decay to top quarks at hadron colliders*, *Phys.Lett.* **B333** (1994) 126–131, [[hep-ph/9404359](#)].
- [40] M. Spira, *HIGLU and HDECAY: Programs for Higgs boson production at the LHC and Higgs boson decay widths*, *Nucl.Instrum.Meth.* **A389** (1997) 357–360, [[hep-ph/9610350](#)].
- [41] R. Harlander and P. Kant, *Higgs production and decay: Analytic results at next-to-leading order QCD*, *JHEP* **0512** (2005) 015, [[hep-ph/0509189](#)].

- [42] K. Chetyrkin and A. Kwiatkowski, *Second order QCD corrections to scalar and pseudoscalar Higgs decays into massive bottom quarks*, *Nucl.Phys.* **B461** (1996) 3–18, [[hep-ph/9505358](#)].
- [43] M. Spira, *QCD effects in Higgs physics*, *Fortsch.Phys.* **46** (1998) 203–284, [[hep-ph/9705337](#)].
- [44] R. V. Harlander, S. Liebler, and H. Mantler, *SusHi: A program for the calculation of Higgs production in gluon fusion and bottom-quark annihilation in the Standard Model and the MSSM*, *Comput.Phys.Commun.* **184** (2013) 1605–1617, [[arXiv:1212.3249](#)].
- [45] J. Alwall, R. Frederix, S. Frixione, V. Hirschi, F. Maltoni, et al., *The automated computation of tree-level and next-to-leading order differential cross sections, and their matching to parton shower simulations*, *JHEP* **1407** (2014) 079, [[1405.0301](#)].
- [46] **LHC Higgs Cross Section Working Group** Collaboration, S. Dittmaier et al., *Handbook of LHC Higgs Cross Sections: 1. Inclusive Observables*, [arXiv:1101.0593](#).
- [47] A. Djouadi, *The Anatomy of electro-weak symmetry breaking. II. The Higgs bosons in the minimal supersymmetric model*, *Phys.Rept.* **459** (2008) 1–241, [[hep-ph/0503173](#)].
- [48] **ATLAS** Collaboration, G. Aad et al., *Search for Scalar Diphoton Resonances in the Mass Range 65 – 600 GeV with the ATLAS Detector in pp Collision Data at $\sqrt{s} = 8$ TeV*, *Phys.Rev.Lett.* **113** (2014), no. 17 171801, [[arXiv:1407.6583](#)].
- [49] **CMS** Collaboration, CMS, “Search for an Higgs Like resonance in the diphoton mass spectra above 150 GeV with 8 TeV data.” CMS-PAS-HIG-14-006, 2014.
- [50] **ATLAS** Collaboration, G. Aad et al., *Search For Higgs Boson Pair Production in the $\gamma\gamma b\bar{b}$ Final State using pp Collision Data at $\sqrt{s} = 8$ TeV from the ATLAS Detector*, *Phys.Rev.Lett.* **114** (2015), no. 8 081802, [[arXiv:1406.5053](#)].
- [51] **CMS** Collaboration, V. Khachatryan et al., *Search for resonant pair production of Higgs bosons decaying to two bottom quark-antiquark pairs in proton-proton collisions at 8 TeV*, [arXiv:1503.04114](#).
- [52] **CMS** Collaboration, CMS, “Search for the resonant production of two Higgs bosons in the final state with two photons and two bottom quarks.” CMS-PAS-HIG-13-032, 2014.
- [53] **ATLAS** Collaboration, *Measurements of the properties of the Higgs-like boson in the four lepton decay channel with the ATLAS detector using 25 fb⁻¹ of proton-proton collision data*, .
- [54] A. Martin, W. Stirling, R. Thorne, and G. Watt, *Parton distributions for the LHC*, *Eur.Phys.J.* **C63** (2009) 189–285, [[arXiv:0901.0002](#)].
- [55] T. Sjostrand, S. Mrenna, and P. Z. Skands, *PYTHIA 6.4 Physics and Manual*, *JHEP* **0605** (2006) 026, [[hep-ph/0603175](#)].
- [56] **DELPHES 3** Collaboration, J. de Favereau et al., *DELPHES 3, A modular framework for fast simulation of a generic collider experiment*, *JHEP* **1402** (2014) 057, [[1307.6346](#)].
- [57] M. Cacciari, G. P. Salam, and G. Soyez, *FastJet User Manual*, *Eur.Phys.J.* **C72** (2012) 1896, [[arXiv:1111.6097](#)].
- [58] **CMS** Collaboration, *Search for supersymmetry in pp collisions at $\sqrt{s} = 8$ TeV in events with three leptons and at least one b-tagged jet*, Tech. Rep. CMS-PAS-SUS-13-008, CERN, Geneva, 2013.

- [59] J. Pumplin, D. Stump, J. Huston, H. Lai, P. M. Nadolsky, et al., *New generation of parton distributions with uncertainties from global QCD analysis*, *JHEP* **0207** (2002) 012, [[hep-ph/0201195](#)].
- [60] **CMS** Collaboration, *Projected Performance of an Upgraded CMS Detector at the LHC and HL-LHC: Contribution to the Snowmass Process*, [1307.7135](#).
- [61] **CMS** Collaboration, *Measurement of the cross section ratio $t\bar{b}b/t\bar{t}j$ in pp Collisions at 8 TeV*, Tech. Rep. CMS-PAS-TOP-13-010, CERN, Geneva, 2013.
- [62] G. Cowan, K. Cranmer, E. Gross, and O. Vitells, *Asymptotic formulae for likelihood-based tests of new physics*, *Eur.Phys.J.* **C71** (2011) 1554, [[arXiv:1007.1727](#)].
- [63] F. Maltoni, K. Paul, T. Stelzer, and S. Willenbrock, *Associated production of Higgs and single top at hadron colliders*, *Phys.Rev.* **D64** (2001) 094023, [[hep-ph/0106293](#)].
- [64] F. Demartin, F. Maltoni, K. Mawatari, and M. Zaro, *Higgs production in association with a single top quark at the LHC*, [arXiv:1504.00611](#).
- [65] *Search for an Invisibly Decaying Higgs Boson Produced via Vector Boson Fusion in pp Collisions at $\sqrt{s} = 8$ TeV using the ATLAS Detector at the LHC*, Tech. Rep. ATLAS-CONF-2015-004, CERN, Geneva, Mar, 2015.
- [66] **ATLAS** Collaboration, G. Aad et al., *Search for direct third-generation squark pair production in final states with missing transverse momentum and two b-jets in $\sqrt{s} = 8$ TeV pp collisions with the ATLAS detector*, *JHEP* **1310** (2013) 189, [[arXiv:1308.2631](#)].
- [67] M. R. Buckley, D. Feld, and D. Goncalves, *Scalar Simplified Models for Dark Matter*, *Phys.Rev.* **D91** (2015), no. 1 015017, [[arXiv:1410.6497](#)].
- [68] **ATLAS** Collaboration, G. Aad et al., *Search for dark matter in events with heavy quarks and missing transverse momentum in pp collisions with the ATLAS detector*, *Eur.Phys.J.* **C75** (2015), no. 2 92, [[arXiv:1410.4031](#)].
- [69] N. Zhou, Z. Khechadorian, D. Whiteson, and T. M. Tait, *Bounds on invisible Higgs boson decay extracted from LHC $t\bar{t}H$ production data*, *Phys.Rev.Lett.* **113** (2014) 151801, [[arXiv:1408.0011](#)].
- [70] **CMS** Collaboration, S. Chatrchyan et al., *Search for top-squark pair production in the single-lepton final state in pp collisions at $\sqrt{s} = 8$ TeV*, *Eur.Phys.J.* **C73** (2013), no. 12 2677, [[arXiv:1308.1586](#)].
- [71] U. Haisch and E. Re, *Simplified dark matter top-quark interactions at the LHC*, [arXiv:1503.00691](#).
- [72] *Prospects for benchmark Supersymmetry searches at the high luminosity LHC with the ATLAS Detector*, Tech. Rep. ATL-PHYS-PUB-2013-011, CERN, Geneva, Sep, 2013.
- [73] M. Carena, S. Heinemeyer, O. Stl, C. Wagner, and G. Weiglein, *MSSM Higgs Boson Searches at the LHC: Benchmark Scenarios after the Discovery of a Higgs-like Particle*, *Eur.Phys.J.* **C73** (2013), no. 9 2552, [[arXiv:1302.7033](#)].
- [74] **LUX** Collaboration, D. Akerib et al., *First results from the LUX dark matter experiment at the Sanford Underground Research Facility*, *Phys.Rev.Lett.* **112** (2014) 091303, [[arXiv:1310.8214](#)].

- [75] P. Huang and C. E. M. Wagner, *Blind Spots for neutralino Dark Matter in the MSSM with an intermediate m_A* , *Phys.Rev.* **D90** (2014), no. 1 015018, [[arXiv:1404.0392](#)].
- [76] P. Harris, V. V. Khoze, M. Spannowsky, and C. Williams, *Constraining Dark Sectors at Colliders: Beyond the Effective Theory Approach*, *Phys.Rev.* **D91** (2015), no. 5 055009, [[arXiv:1411.0535](#)].
- [77] D. R. Tovey, *On measuring the masses of pair-produced semi-invisibly decaying particles at hadron colliders*, *JHEP* **0804** (2008) 034, [[arXiv:0802.2879](#)].
- [78] G. Polesello and D. R. Tovey, *Supersymmetric particle mass measurement with the boost-corrected contranverse mass*, *JHEP* **1003** (2010) 030, [[arXiv:0910.0174](#)].
- [79] B. Field, S. Dawson, and J. Smith, *Scalar and pseudoscalar Higgs boson plus one jet production at the CERN LHC and Tevatron*, *Phys.Rev.* **D69** (2004) 074013, [[hep-ph/0311199](#)].
- [80] Y. Bai, H.-C. Cheng, J. Gallicchio, and J. Gu, *Stop the Top Background of the Stop Search*, *JHEP* **1207** (2012) 110, [[arXiv:1203.4813](#)].
- [81] K. A. Assamagan and N. Gollub, *The ATLAS discovery potential for a heavy charged Higgs boson in $gg \rightarrow tbH^{\pm}$ with $H^{\pm} \rightarrow tb$* , *Eur.Phys.J.* **C39S2** (2005) 25–40, [[hep-ph/0406013](#)].
- [82] X. Gong, Z.-G. Si, S. Yang, and Y.-j. Zheng, *Top quark spin and Htb interaction in charged Higgs boson and top quark associated production at LHC*, *Phys.Rev.* **D87** (2013), no. 3 035014, [[arXiv:1210.7822](#)].
- [83] Q.-H. Cao, X. Wan, X.-p. Wang, and S.-h. Zhu, *Searching for Charged Higgs Boson in Polarized Top Quark*, *Phys.Rev.* **D87** (2013), no. 5 055022, [[arXiv:1301.6608](#)].
- [84] X. Gong, Z.-G. Si, S. Yang, and Y.-J. Zheng, *Determination of charged Higgs couplings at the LHC*, *Mod.Phys.Lett.* **A29** (2014) 1430013, [[arXiv:1404.1545](#)].
- [85] W. Xiao-ping and Z. Shou-hua, *On Extra Neutral and Charged Higgs bosons at the LHC*, [[arXiv:1405.1800](#)].
- [86] **ATLAS** Collaboration, G. Aad et al., *Search for the $b\bar{b}$ decay of the Standard Model Higgs boson in associated $(W/Z)H$ production with the ATLAS detector*, *JHEP* **1501** (2015) 069, [[arXiv:1409.6212](#)].
- [87] **ATLAS** Collaboration, G. Aad et al., *Search for the Standard Model Higgs boson produced in association with top quarks and decaying to $b\bar{b}$ in pp collisions at $\sqrt{s} = 8$ TeV with the ATLAS detector at the LHC*, .
- [88] **ATLAS** Collaboration, G. Aad et al., *Evidence for Higgs boson Yukawa couplings in the $H \rightarrow \tau\tau$ decay mode with the ATLAS detector*, .
- [89] **ATLAS** Collaboration, G. Aad et al., *Observation and measurement of Higgs boson decays to WW^* with ATLAS at the LHC*, .
- [90] **ATLAS** Collaboration, G. Aad et al., *Measurements of Higgs boson production and couplings in the four-lepton channel in pp collisions at center-of-mass energies of 7 and 8 TeV with the ATLAS detector*, *Phys.Rev.* **D91** (2015), no. 1 012006, [[arXiv:1408.5191](#)].
- [91] **ATLAS** Collaboration, G. Aad et al., *Measurement of Higgs boson production in the diphoton decay channel in pp collisions at center-of-mass energies of 7 and 8 TeV with the ATLAS detector*, *Phys.Rev.* **D90** (2014), no. 11 112015, [[arXiv:1408.7084](#)].

- [92] **CMS** Collaboration, *Precise determination of the mass of the Higgs boson and studies of the compatibility of its couplings with the standard model*, .
- [93] **CMS** Collaboration, *Search for $t\bar{t}H$ production using the Matrix Element Method*, .
- [94] **CMS** Collaboration, V. Khachatryan et al., *Observation of the diphoton decay of the Higgs boson and measurement of its properties*, *Eur.Phys.J.* **C74** (2014), no. 10 3076, [[arXiv:1407.0558](https://arxiv.org/abs/1407.0558)].